Application of quantitative MRI methods in central nervous system diseases

Ph.D. thesis

Szilvia Anett Nagy

Supervisor:
Prof. Péter Bogner, M.D., Ph.D.

Leader of Doctoral Program:
Prof. Péter Bogner, M.D., Ph.D.

Leader of Doctoral School:
Prof. Sámuel Komoly, M.D., D.Sc.

University of Pécs
Doctoral School of Clinical Neuroscience
Pécs, 2017

Table of contents

Abbreviations

^{1}H-MRS	Proton magnetic resonance spectroscopy
AAO	Age at epilepsy onset
ADC	Apparent diffusion coefficient
ADC_f	Fast diffusion component
ADCs	Slow diffusion component
BET	FMRIB's Software Library Brain extraction tool
CNS	Central nervous system
CPMG	Carr-Purcell-Meiboom-Gill
DD	Disease duration
DWI	Diffusion-weighted imaging
EDSS	Expanded Disability Status Scale
EEG	Electroencephalogram
EPI	Echo-planar imaging
FAST	FMRIB's Automated Segmentation Tool
f_f	Volume fraction of fast diffusion component
FLAIR	fluid attenuated inversion recovery
FLIRT	FMRIB's Linear Image Registration Tool
FNIRT	FMRIB's Nonlinear Image Registration Tool
FOV	Field of view
FSL	FMRIB Software Library
f_s	Volume fraction of slow diffusion component
GM	Grey matter
TI	Inversion time
IVDD	Intervertebral disc degeneration
MPRAGE	magnetization-prepared rapid acquisition with gradient echo
MRI	Magnetic resonance imaging
MS	Multiple sclerosis
MTLE-HS	mesial-temporal lobe epilepsy with unilateral hippocampal sclerosis
MTR	Magnetization transfer ratio

NAWM	Normal appearing white matter
NIfTI	Neuroimaging Informatics Technology Initiative
NP	Nucleus pulposus
RF	Radiofrequency
ROI	Region of interest
SNR	Signal to noise ratio
TE	Echo time
TLN	Total lesion number
TLV	Total lesion volume
TR	Repetition time
WM	White matter

1. General introduction – quantitative approaches of MRI signal decay

During the past couple of decades, conventional magnetic resonance imaging (MRI) techniques have been increasingly used to assess alterations in the central nervous system (CNS). Nowadays, a variety of conventional MRI protocols are also routinely used to detect therapeutic effects of different treatment strategies. These offer several important advantages, such as the definition of disability level, the association of blood brain barrier damage, spatial and temporal dissemination of brain lesions. In the past few years, a host of non-conventional quantitative MRI techniques have been introduced for the assessment of CNS diseases. These MRI techniques appear to be reliable markers in monitoring pathologic processes related to disease activity and clinical progression. They are able to reveal a range of tissue changes that include oedema, inflammation, demyelination, axonal loss, and degeneration. Therefore, in a disease with a high degree of longitudinal variability of clinical signs and with no current adequate biological markers of disease progression, non-conventional quantitative MRI techniques provide a powerful tool to non-invasively investigate not only the pathological substrates of overt lesions but also subtle global changes that may affect the entire brain. Additionally, conventional MR imaging gives only a cross-sectional qualitative information of different tissues, while quantitative approaches offer the advantage of absolute rather than relative characterization of the underlying biochemical composition of the tissue. The determination of quantitative MRI data requires more detailed approaches and a good understanding of basic MR phenomena. Generally, it is performed by using and analysing a set of qualitative images, where the signal intensity is controlled by the change of an MR imaging parameter: inversion time (TI), flip angle or repetition time (TR) for T1 relaxometry; echo time (TE) for T2 relaxometry and b-value for diffusion-weighted data. Then quantitative MR data can be calculated by mono- or multi-exponentially fitting the signal change against these parameters (see corresponding sections of Technical background). In clinical perspective, T1 and T2 relaxation times depend on structural characteristics such as local tissue density (i.e. water content), while quantitative diffusion data provides an indirect measure of tissue structure on a microscopic scale.

Taking the advantage of quantitative MRI techniques, a series of studies tested the usefulness of them in the CNS where conventional MR methods were insensitive. MR

imaging of the CNS has great importance in the diagnostic evaluation and monitoring of treatment response in multiple sclerosis (MS) (Wattjes et al., 2015). Also mild traumatic brain injury patients with negative computed tomography scans showed significant alterations on advanced quantitative MR images (Toth et al., 2013). Additionally, numerous studies of lesional and non-lesional epilepsy patients have demonstrated that advanced quantitative MRI methods can reliably improve surgical outcome (Wehner and Luders, 2008) and help the detection of seizure origin. Although white matter (WM) alterations with distinct lesions-tissue contrast are still the main radiological hallmark in many of CNS diseases, the detection of pathological WM without visible contrast changes is also important and even more challenging.

1.1.The examination of normal appearing white matter

It is known that some pathologies in CNS cannot be perceived on conventional (T1- and T2-weighted) MR images. In such cases, signal intensity is not altered focally, rather changed homogenously, but in a minor extent (Bakshi et al., 2008). Quantitative MRI methods are suitable for measuring changes that are not straightforward for the human visual perception (Beaulieu et al., 1998; Jones et al., 2003; Whittall et al., 1997). Diffusion imaging is a quantitative method of choice to delineate microstructural changes in the brain tissue (de Carvalho Rangel et al., 2011). Tissue water diffusion changes in the WM were demonstrated during normal development and aging of the human brain (Camara et al., 2007; Forbes et al., 2002; Naganawa et al., 2003; Sala et al., 2012). Myelin content of the brain increases in the first few years of life; thereafter significantly decreases with aging (Malone and Szoke, 1982; Marner et al., 2003). It appears that reduced myelin content results in increased tissue water diffusion, as it was measured either in new-born or in aging brain (Barkovich, 2000; Forbes et al., 2002). Similar diffusion changes were described in pathological conditions that affect myelinated structures (Bakshi et al., 2008; Caramia et al., 2002). The increased tissue water diffusion in WM structures of MS patients depends on several conditions, e.g. the subtype of MS, the time course of inflammation, demyelination and remyelination, lesion volume, etc. (Caramia et al., 2002; Garaci et al., 2007; Meier et al., 2007; Miller et al., 2003; Schmierer et al., 2004). According to previous studies, MS causes widespread tissue damage in the normal appearing white matter (NAWM) of the brain and the spinal cord, whose extent and severity are more strictly associated with clinical manifestations of the disease than the

extent of focal pathology (Filippi and Rocca, 2005). In addition, loss of cellular elements changes the ratio of intra-extracellular compartments that also contributes to the increase of tissue water diffusion (Moore et al., 2008; Sala et al., 2012). Parameters obtained from the water diffusion tensor, such as fractional anisotropy and mean diffusivity, can demonstrate alterations in axonal microstructure. Further potential MRI biomarkers of WM damage are the magnetization transfer ratio (MTR) and the longitudinal relaxation time (T1 relaxometry) measurements. MTR can show pathologic alterations in WM that involve macromolecules in the cell membrane, such as in inflammation or in demyelination (Fazekas et al., 2005). T1 relaxometry provides quantitative information on brain water content and is therefore a potential marker for oedematous brain tissue (Bastin et al., 2002). Additionally, substantial evidence exists for prolonged T2 in damaged but visually normal WM compared to the WM of healthy volunteers (Whittall et al., 2002), while proton MR spectroscopy (^{1}H-MRS) can add information on the biochemical nature of such changes. In mesial-temporal lobe epilepsy, it is known that structural abnormalities associated with hippocampal sclerosis involve not only the hippocampus and the structures of the limbic system (Baldwin et al., 1994; Cendes et al., 1993; Mamourian and Brown, 1993; Van Paesschen et al., 1996) but also the bilateral WM with ipsilateral predominance (Concha et al., 2009; Concha et al., 2005; Flugel et al., 2006; Focke et al., 2008; Gross et al., 2006; Hermann et al., 2002; Kim et al., 2008; Lin et al., 2008; Riley et al., 2010; Seidenberg et al., 2005). It might be hypothesized that neuronal dysfunction/loss in the sclerotic hippocampus causes damage to WM structures connected to the epileptic foci because of the excitotoxic effects of the spreading epileptogenic activity which then induces microstructural abnormalities far away from the seizure focus (Scanlon et al., 2013; Seidenberg et al., 2005).

1.2.Quantitative MRI of intervertebral disc degeneration

Most of the quantitative MRI techniques have been validated and applied in the brain over the past 20 years, but quantitative MRI of the spine is underutilized both in research and in the clinical practice. This is a direct consequence of the difficulties related to the numerous artefacts and image quality. Thanks to recent developments in a number of areas including coils, acquisition protocols and image processing techniques, quantitative spinal MR imaging had continuously been improved and overcame most of the challenges. To date, numerous studies and books exist to study

how to apply these techniques in the spinal cord (Cohen-Adad and Wheeler-Kingshott, 2014), but fewer examined the quantitative MRI alterations in intervertebral disc diseases, although low back pain is one of the most prevalent and costly illness in today's society. Early signs of disc degeneration are manifested by biophysical and biochemical changes, including loss of proteoglycans, osmotic pressure and hydration (Adams and Roughley, 2006). Quantitative MRI has the potential to become an important diagnostic and treatment assessment tool in determining the functional state of intervertebral disc matrix.

Several MRI grading systems have been used to characterize intervertebral disc degeneration (IVDD) in humans. Most classification systems for IVDD focus on the signal intensity and morphology of the nucleus pulposus (NP) on sagittal T2-weighted MR images (Griffith et al., 2007; Gunzburg et al., 1992; Kanayama et al., 2009; Pfirrmann et al., 2001; Schneiderman et al., 1987; Tertti et al., 1991), because the decreased signal intensity correlates with the degree of the degenerative process, including the loss of water and proteoglycan content (Haneder et al., 2013). Currently, the most widely accepted grading system was described by Pfirrmann et al. which is based on the distinction between the signal intensity of the NP and annulus fibrosus, disc structure and disc height (Pfirrmann et al., 2001). Other grading system such as Schneiderman scheme also provides a reliable method to measure the degeneration of the disc (Schneiderman et al., 1987). However, morphology-based grading of IVDD suffers from two substantial shortcomings. Firstly, the T2 process might be affected by several molecular events that result in subtle signal intensity changes of the NP. Secondly, the visual perception of intensity changes on T2W images is problematic due to many arbitrary factors in signal detection and amplification. These may lead to significant differences between observers causing interobserver bias, especially when observers classify minor changes. The disparity between observers in terms of rating behaviour is mostly due to the consistent over or underestimation of the grading boundaries. Based on the biophysical and biochemical changes in discs, several MR imaging techniques have been developed for quantitative evaluation of IVDD, such as magnetization transfer imaging (Paajanen et al., 1994; Wang et al., 2010), T1 and T1rho imaging (Jenkins et al., 1985; Nguyen et al., 2008; Zobel et al., 2012), ^{1}H-MRS (Zuo et al., 2009), diffusion-weighted imaging (DWI) (Beattie et al., 2008; Niinimaki et al., 2009), and T2 measurements (Marinelli et al., 2010; Perry et al., 2006). T1rho relaxation measurement – which probes the interaction between water molecules and

their macromolecular environment – is suggested to have the potential to identify early biochemical changes in the intervertebral disc. In cadaveric human discs it was shown that T1rho strongly correlates with proteoglycan content in the NP (Johannessen et al., 2006). Additionally, chemical exchange saturation transfer and MTR may also offer promise for more accurately discriminating between discs of different health (Schleich et al., 2016; Wang et al., 2010). Recently developed quantitative T2* relaxometry seems to be an emerging technique with the additional benefit of three-dimensionality in providing information about spatial macromolecule architecture in conjunction with water molecule mobility (Ellingson et al., 2013). Among these methods, T2 relaxation time evaluation provides a reliable correlation to detect changes in the molecular environment of the disc (Trattnig et al., 2010) and the method is implemented on most clinical MR scanners. T2 relaxation time measurements correlate with intervertebral disc tissue water content (Marinelli et al., 2009) and have therefore been used to quantify the hydration of the disc which is essential for disease grading (Jazini et al., 2012; Takashima et al., 2012).

2. Technical background

2.1. Diffusion imaging

In 1827, the Scottish botanist Robert Brown noticed that pollen grains suspended in water showed random (or Brownian) motion. Due to density differences in a system, Brownian motion is driven by the concentration gradients. The transport of material in stagnant fluid or across streamlines in a laminar flow can be explained by molecular diffusion described by Fick's first law. This law relates the flux to the concentration under the assumption of steady state. It postulates that the flux *(J)* goes from regions with high concentration to low concentration, with a magnitude that is proportional to the concentration gradient (E.q. 1).

$$J = -D \cdot \frac{\Delta c}{\Delta x} \qquad \text{E.q. 1}$$

where D is the diffusion coefficient, while $\Delta c/\Delta x$ is the concentration change as a function of distance. When D is known, the microscopic transport of a material can be described using Einstein diffusion equation:

$$\Delta r^2 = 2 \cdot D \cdot t \qquad \text{E.q. 2}$$

Here the mean square displacement (Δr^2) of a particle per unit time (Δt) is expressed along one direction. If a glass of water at constant temperature is considered, the diffusion is only affected by collisions between particles and the wall, therefore the self-diffusion (D) is in steady state. The average displacement of pure water at body temperature (37 °C) is much greater – during an 50 ms motion interval is approximately 30 μm (Norris, 2001) – compared to the dimension of cells. If the diffusing water molecules encounter any barriers along their random walk motion, the mean square displacement per unit time will be lower than in pure water. In the brain, water molecules interact with many tissue components, such as cell membranes, cell organelles or macromolecules and the indirect observation of these displacements provides valuable information on the microscopic barriers. For instance, in the grey matter (GM) the cellular membranes are not oriented along a specific direction; therefore the water diffusion is isotropic or equal in all paths. In the WM, diffusion is faster parallel to the fibres, hence the diffusion is anisotropic.

Also the distribution of water is different in the extracellular and the intracellular spaces. Normally, the largest amount of water diffusion takes place in the extracellular space, while restriction effects, high viscosity, macromolecular crowding and cell membranes explain the reduction of water diffusion intracellularly.

2.1.1. Diffusion-weighted MRI

Up to date, Stejskal-Tanner sequence is the most widely used approach to detect random motion of water molecules in the body. In this sequence, two diffusion-encoding gradients (dephasing and rephasing) in matched pairs are placed on both sides of the 180° radiofrequency (RF) pulse (Figure 1).

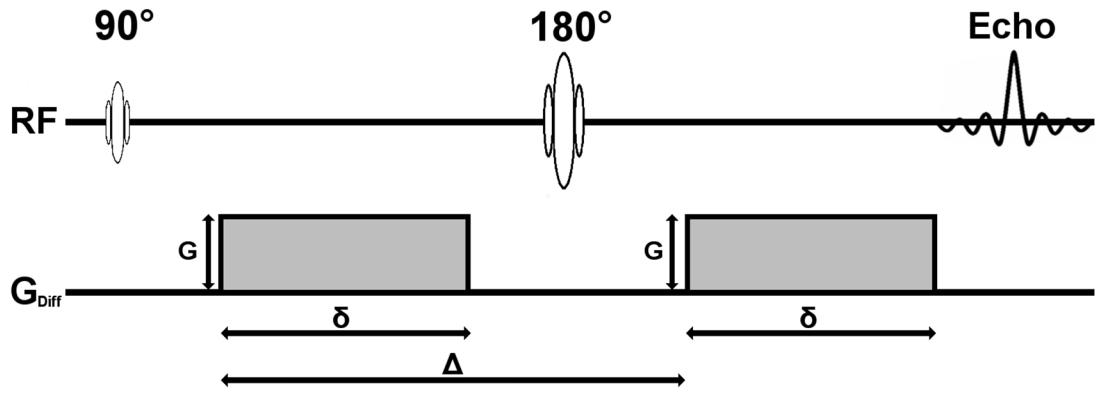

Figure 1. The schematic representation of Stejskal-Tanner pulsed gradient spin-echo scheme.

In a static system characterized by homogeneous magnetic field, all protons have the same precession frequency. However, if the dephasing gradient is turned on, this homogeneity will be disturbed resulting in signal loss. This gradient is followed by another with opposite direction (i.e. rephasing gradient) and the signal will be restored. If the localization of protons change between dephasing and rephasing the signal recovery will be incomplete. Since the spins are not stationary, the longer the observation time, the greater the spread of spin positions (due to diffusivity). MRI can be sensitized to diffusion, where the strength of diffusion weighting is dependent on the duration of time between the dephasing and rephasing gradients (Δ), the gyromagnetic ratio (γ), the gradient strength (G) and its duration (δ) which is summarized in the so called b-value (E.q. 3) (Gillard et al., 2009).

$$b = \gamma^2 \cdot G^2 \cdot \delta^2\left(\Delta - \frac{\delta}{3}\right) \qquad \text{E.q. 3}$$

The resulting diffusion-weighted signal intensity can be easily determined using the following equation (E.q. 4):

$$I = I_0 \cdot e^{(-b \cdot ADC)}, \qquad \text{E.q. 4}$$

where I is the measured signal intensity with diffusion sensitization, I_0 is the signal intensity without diffusion sensitization, b is the b-value (unit s/mm^2) and ADC is the

apparent diffusion coefficient. *ADC* can be estimated using E.q. 4 by acquiring at least two signals with different b-values. However, if the diffusion-weighted image is acquired in a single diffusion direction only, then anisotropy can strongly influence the results. As a remedy, DWI is acquired in three orthogonal directions and then the geometric mean is taken to create the so called trace image.

2.1.2. Multi-exponential diffusion signal decay

The signal decays mono-exponentially in freely diffusing systems, however if the motion of water is restricted by barriers such as cell walls, membranes and intracellular organs, the measured diffusion will be partially reduced resulting a non mono-exponential signal decay (Figure 2).

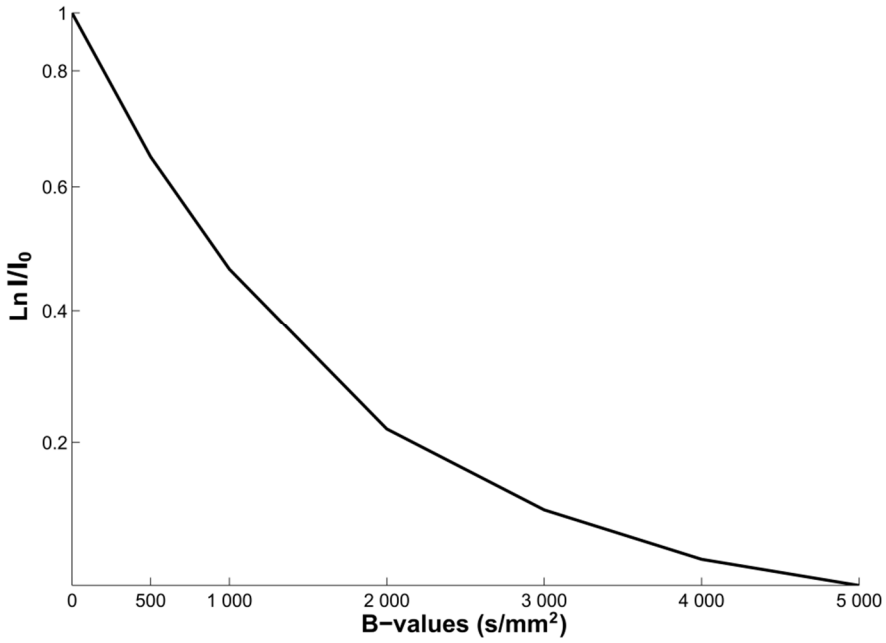

Figure 2. The representation of diffusion related data fitting using a non mono-exponential approach.

In biological systems, one often finds that the signal decay with increasing b-value can be expressed as a sum of multiple-exponentials. A common interpretation is that the observed signal contains multiple compartments with different sizes and shapes (Milne and Conradi, 2009). However, Sukstanskii et al. (Sukstanskii et al., 2003) showed that, even in single-compartments, the signal is not mono-exponential but can be well modelled bi-exponentially (E.q. 5).

$$\frac{I}{I_0} = f_{fast} \cdot e^{(-b \cdot ADC_{fast})} + f_{slow} \cdot e^{(-b \cdot ADC_{slow})} \qquad \text{E.q. 5}$$

Bi-exponential decay corresponds to two water diffusion pools and described with fast (ADC_{fast}) and slow (ADC_{slow}) diffusion components (Assaf and Cohen, 1998; Niendorf et al., 1996). Here, f is the volume fraction associated with the fast and the slow diffusion phases, where f_{fast}=1-f_{slow}. Some studies demonstrated that, fast diffusion component gives about 65% of the diffusion signal in the normal brain (Niendorf et al., 1996). At relatively low b-values, signal intensity is dominated by fast diffusion component, whereas it is contributed mainly by slow diffusion component at high b-values (Figure 3) (DeLano et al., 2000).

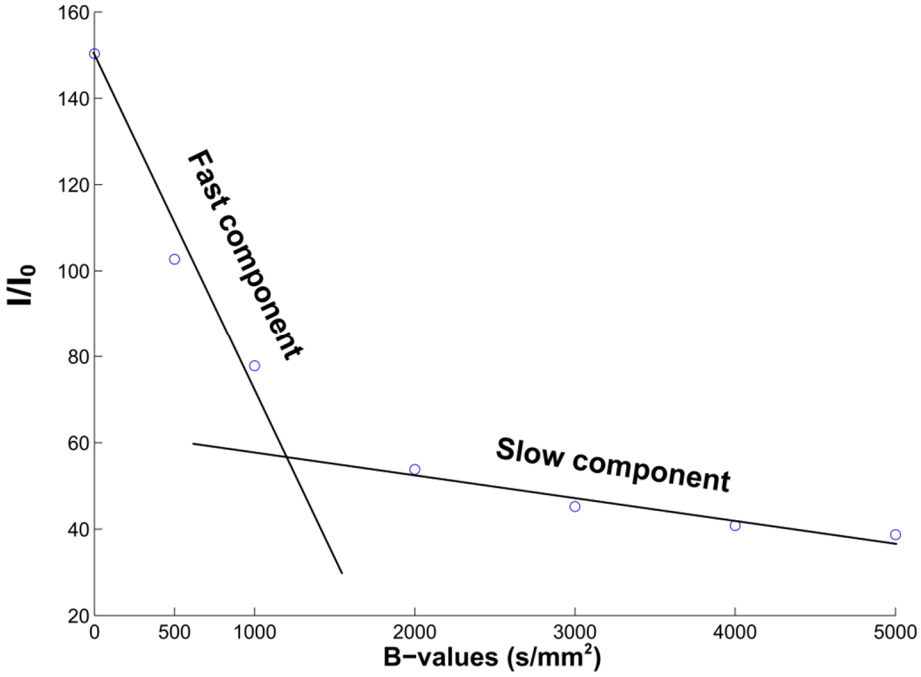

Figure 3. The simulation of fast and slow diffusion components contributing to DWI signal.

Although the contribution of fast and slow diffusion components to body fluid compartments is unclear, it was suggested that extracellular compartment might correspond to fast diffusion component, because water expected to diffuse more rapidly than in the intracellular space (Le Bihan and van Zijl, 2002). Further works showed that, bi-exponential behaviour could also be seen in the intracellular compartment confirming that both slow and fast diffusion components coexist intracellularly, while the variations in size of the intracellular and the extracellular compartments correlate with the changes of the fraction of the slow and the fast diffusion components (Niendorf et al., 1996; van der Toorn et al., 1996).

2.2. T2 relaxometry

The theory of relaxometry, or the measurement of relaxation rates, is based on the physical aspects of nuclei relaxation to the ground state after being excited by an RF pulse. More specifically, T2 relaxation is the decay of transverse components of magnetization produced by randomly occurring variations in the local magnetic field strength. It begins immediately after the RF pulse and protons start to become out of phase as they experience a slightly different magnetic field. This transverse relaxation occurs due to magnetic field inhomogeneities and movement of the molecules in the tissue. In clinical practice the evaluation of T2 relaxation process of different tissue types is based on the correctly chosen tissue specific weighting parameter (TE). However, this process shows only a cross sectional information of the weighting procedure and the whole relaxation course remains unknown and no quantitative information can be determined. In order to address this limitation, a set of T2-weighted images are obtained at different TEs, which is now called T2 relaxometry.

2.2.1. Image acquisition methods

A variety of acquisition methods exist to measure T2 relaxation time in a certain tissue. The simplest and most widely available approach is a single or Hahn spin echo sequence. This applies a 90° (excitation) and a 180° (refocusing) pulse and repeats the acquisition for different echoes. This is the most accurate method of T2 quantification but its long scanning duration is impractical for clinical studies. To save time, multiple spin echo approach using multiple refocusing pulses shortens the acquisition length, but its accuracy is compromised by imperfect RF pulses. The Carr-Purcell-Meiboom-Gill (CPMG) sequence is a modification of this approach (Figure 4) where 90° phase shift in the rotating frame of reference was applied between the 90° and the subsequent 180° pulses in order to reduce accumulating effects of imperfections in the 180° pulses.

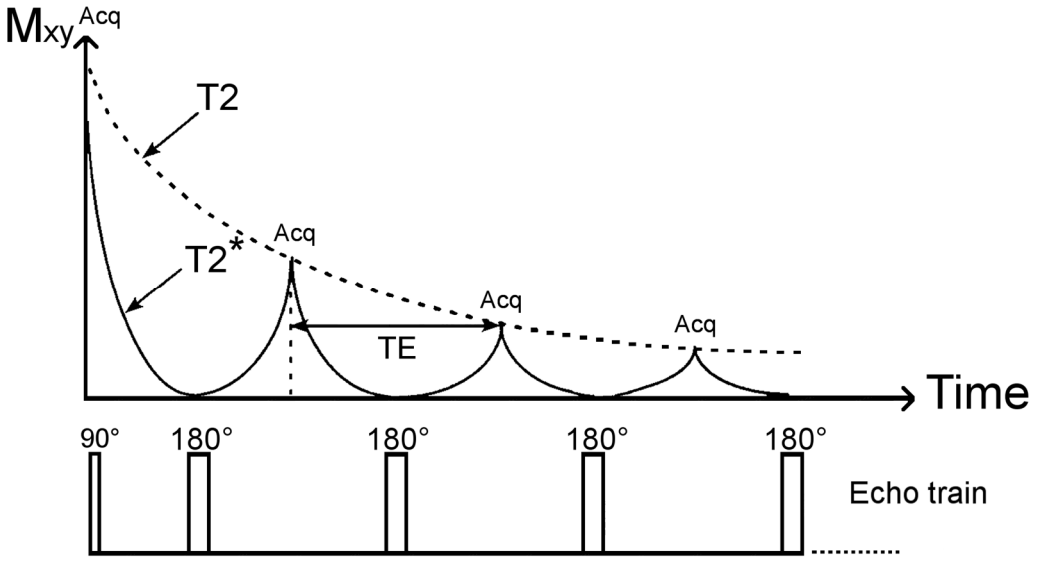

Figure 4. The schematic representation of CPMG sequence.

However, CPMG sequence still has been found to be insufficient for accurate multi-slice T2 determination (Majumdar et al., 1986) due to residual sensitivity to refocusing imperfections called stimulated echoes. To minimize the effect of that, optimized refocusing pulses can be used (Lebel and Wilman, 2010) or data points can be excluded from the fitting procedure (Milford et al., 2015). To sum up, the sensitivity of T2 relaxometry depends on the applied sequence, the TR, the TEs, the number of images acquired with different TEs (echo train length) and on the model adopted for fitting the experimental data.

2.2.2. Data processing

To calculate T2 relaxation times of a certain tissue, the raw imaging data acquired with multiple echoes can be fitted via mono- or multi-exponential approaches. Although different quantification methods available (Milford et al., 2015), the use of standard mono-exponential model is still the most frequently applied fitting approach. In order to choose the best fitting procedure for T2 relaxometry, it is worth to first plot the natural logarithm of the signal against TE (Tofts, 2005). The resulting semi logarithmic plot clearly shows whether, there is more than one relaxing component present in the data (Figure 5).

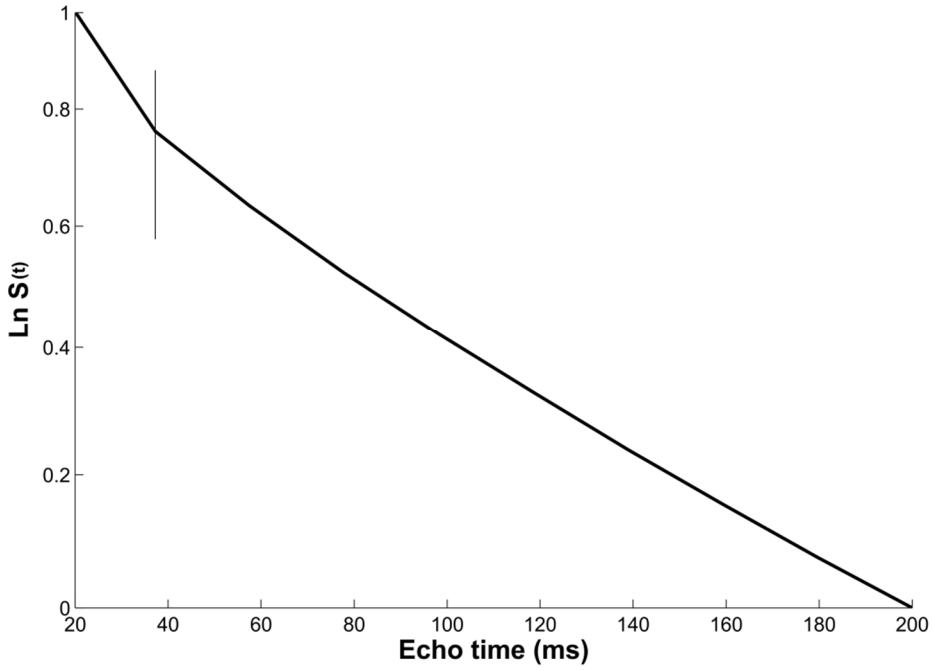

Figure 5. A schematic representation of bi-exponential T2 signal decay on a semi-logarithmic plot.

If no curvature is found, the data analysis approach should be a mono-exponential model (E.q. 6).

$$S = S_0 \cdot e^{(\frac{-TE}{T2})}, \qquad \text{E.q. 6}$$

where S_0 is proportional to the proton density.

If there will be two distinct linear regions to the resulting plot, bi-exponential fitting approach is more reasonable (E.q. 7).

$$S_{(t)} = S_{long} \cdot e^{(-TE/T2_{long})} + S_{short} \cdot e^{(-TE/T2_{short})}, \qquad \text{E.q. 7}$$

where S_{long} and S_{short} are the signals from the long and short T2 components at time zero and $T2_{long}$ and $T2_{short}$ are the long and short T2 relaxation times. This model requires appropriate signal to noise ratio (SNR). If SNR is low, the fit becomes uncertain, reducing the accuracy and precision of the model. In addition, the relaxation times ($T2_{long}$ and $T2_{short}$) should be within an order of magnitude of each other, while S_{long}, and S_{short} should not fall below about 15%. However, it is possible that more than two components are present. In that case it is reasonable to perform a chi-squared test to determine whether or not additional terms need to be added to the model (Armspach

et al., 1991). For both mono- and multi-exponential fitting procedures, nonnegative least square method is suggested to solve the equations (Lawson and Hanson, 1995), but other fitting algorithms exist (Kanzow et al., 2004).

2.3. Applied image processing methods

Many MR image processing tools (e.g. FMRIB Software Library, Freesurfer, 3D Slicer, Statistical Parametric Mapping, HAMMER, Insight Segmentation and Registration Toolkit, etc.) are available to quantitatively analyse MRI data. Most of them are designed to analyse data using both pre- (data conversion, skull stripping, B1 bias field correction, etc.) and post-processing (segmentation, image registration, etc.) steps. However, it is desirable to combine different functions of the processing tools to achieve the desired study specific results.

2.3.1. Pre-processing

In many cases, one of the first pre-processing steps is to convert images from Digital Imaging and Communications in Medicine (DICOM) to Neuroimaging Informatics Technology Initiative (NIfTI) format which is used by most of the image processing tools. NIfTI is a modern incarnation of the Analyze format (where a pair of binary files exist, one containing header and one containing the information of image), but includes important information like the spatial orientation of the image (Whitcher et al., 2011).

As for brain image evaluation, segmentation and registration algorithms work better when tissues external to the brain (i.e. eyeballs, skin, fat, muscle, etc.) are excluded. This process is called brain extraction and it is one of the early pre-processing steps on the initial NIfTI format MR images. The Brain Extraction Tool (BET), provided by FMRIB Software Library (FSL) is a method of choice to eliminate non-brain tissues with highly variable contrast and geometry. Given that FSL was used for most of the data analysis in our studies, we decided to apply BET for brain extraction. The technical details of that were described previously (Smith, 2002). In short, after obtaining a “rough” brain/non-brain threshold, the centre of initial brain surface sphere (centre-of-gravity) is determined. Then a triangular tessellation of a sphere’s surface centred on the centre-of-gravity is initialized and allowed to slowly deform toward the brain’s edge in an iterative process.

To achieve reasonably well results, the performance of BET can be optimized by varying the user-adjustable thresholds (fractional intensity threshold; threshold gradient) and defining the coordinates for centre of initial brain surface sphere. The fractional intensity threshold is changeable from its default value of 0.5 to give smaller (>0.5) or larger (<0.5) brain outline estimates, while the threshold gradient is a valuable option to give a larger brain outline at the bottom of the image and smaller at the top (>0), or vice versa (<0).

2.3.2. Segmentation

Over the last few decades, the enormous development of MR imaging methods has opened a variety of study fields due to high image quality and contrast. The analysis of MR data has become a tedious and complex task for researchers because of the manual extraction of information. Although manual segmentation is often time-consuming and prone to errors, it is still intensively used due to segmentation problem (Birkfellner, 2011). As a consequence, we decided to use manual segmentation in two of our experiments.

Although segmentation is a rather complex and often requiring manual interaction, time-efficient, validated and continuously evolving automated methods have been extensively used especially for brain evaluation.

- ***FSL***

A wide variety of approaches have been proposed for statistical segmentation of brain MR images into different tissue classes (i.e. WM, GM and cerebrospinal fluid), from which parametric ones are most widely employed (Kundu, 1990). These relatively simple methods attempt to determine tissue classes based on probability values estimated from the intensity distribution of the image. However, this approach has an intrinsic limitation that spatial information is not considered. It may work well on images with high contrast and low levels of noise, but these conditions are seldom satisfied for real data, where imperfections such as artefacts, partial volume effect or bias field distortion are present. In order to address these issues, a novel approach developed by Zhang et al. and implemented as FMRIB's Automated Segmentation Tool (FAST) was used in one of our experiments (Zhang et al., 2001). FAST segments the brain based on a hidden Markov random field model and an associated Expectation Maximization algorithm, taking the spatial neighbourhood information into account,

whilst also correcting for the bias field. Various outputs, such as partial volume maps for each class (Figure 6), a single image containing "hard" (binary) segmentation of tissue classes (Figure 7), as well as a restored input image after correction for bias field (Figure 8) are generated.

Figure 6. Partial volume maps for cerebrospinal fluid (A), GM (B) and WM (C), where each voxel has a value from 0 to 1 that represents the fraction of the specific tissue type in that voxel.

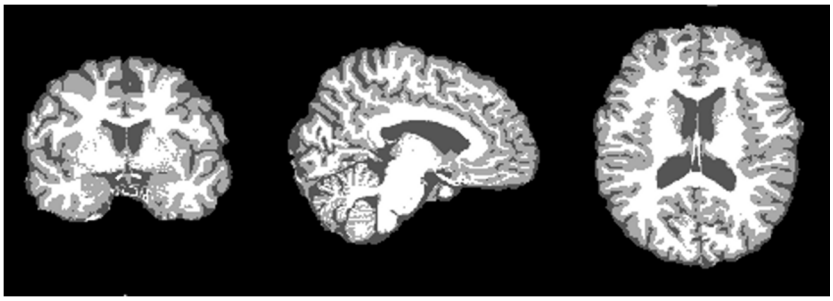

Figure 7. The "hard" (binary) segmentation of tissue classes, where each voxel is classified into only one class, with a value of 1 for cerebrospinal fluid, a value of 2 for GM and a value of 3 for WM.

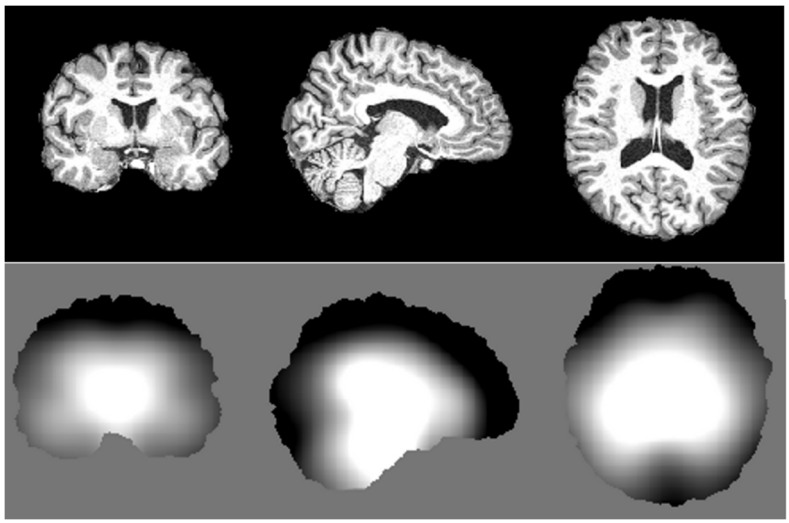

Figure 8. The restored input image of a subject after correction for the bias field (first row) and the estimated bias field (second row).

- ***FreeSurfer***

Another reliable automated method with high accuracy and reproducibility is FreeSurfer software. Given that FreeSurfer was found to be accurate and it is also able to segment each subcortical WM (frontal, parietal, temporal and occipital) lobes, we decided to use FreeSurfer also in our experiment to assess lobar WM differences. Technical details of the automated subcortical segmentation are described in prior publications (Fischl et al., 2002; Fischl et al., 2004).

In brief, the subcortical segmentation stream of FreeSurfer gives automatic segmentation and volumetric data of about 40 brain structures including: left and right cerebral WM, cerebral cortex, lateral ventricle, inferior lateral ventricle, cerebellum WM, cerebellum cortex, thalamus, caudate, putamen, pallidum, hippocampus, amygdala, lesion, accumbens area, ventral diencephalon, vessel, the third ventricle, the fourth ventricle, the brain stem and the cerebrospinal fluid. FreeSurfer applies several pre-processing steps before the segmentation process (Collins et al., 1994; Segonne et al., 2004; Sled et al., 1998). After segmentation, lobar WM is created for each voxel labelled as WM in the aseg file and its label is reassigned to be that of the closest cortical point if its distance is less than 5 mm (Figure 9). Those cortical areas were the following for

- ***Frontal area:*** Superior Frontal, Rostral and Caudal Middle Frontal, Pars Opercularis, Pars Triangularis, Pars Orbitalis, Lateral and Medial Orbitofrontal, Precentral, Paracentral and Frontal Pole regions

– ***Parietal area:*** Superior Parietal, Inferior Parietal, Supramarginal, Postcentral and Precuneus regions

– ***Temporal area:*** Superior, Middle, and Inferior Temporal, Banks of the Superior Temporal Sulcus, Fusiform, Transverse Temporal, Entorhinal, Temporal Pole and Parahippocampal regions

– ***Occipital area:*** Lateral Occipital, Lingual, Cuneus and Pericalcarine regions (https://surfer.nmr.mgh.harvard.edu/fswiki/CorticalParcellation).

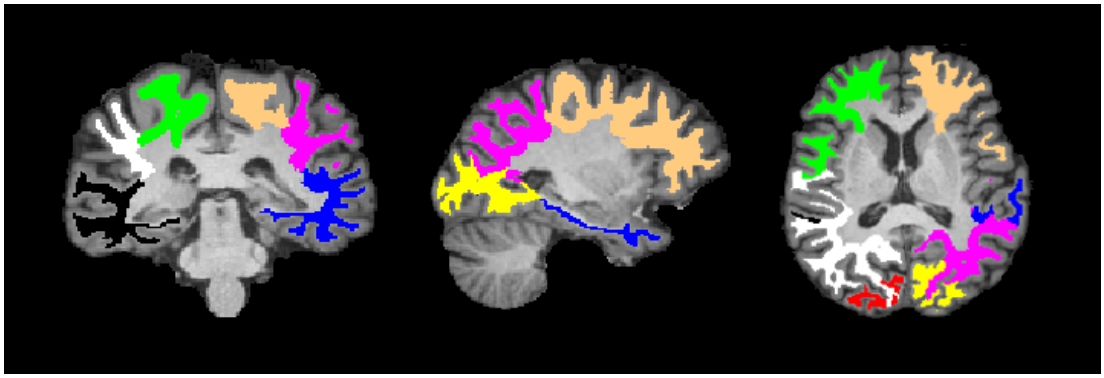

Figure 9. A representative image of lobar WM segmentation derived from FreeSurfer. Black – right temporal WM, white – right parietal WM, red – right occipital WM, green – right frontal WM, blue – left temporal WM, purple – left parietal WM, yellow – left occipital WM, beige – left frontal WM

2.3.3. Registration

To derive (diffusion related) functional information from the automatically segmented brain structures, one further step is required called image registration. Registration algorithms can be divided into linear and nonlinear methods depending on the type of the transformation models. In order to change the position, orientation or shape of the image, a spatial transformation is applied. The transformation model is described using degrees of freedom, which is the number of independent ways that the transformations can be changed. Mathematically, it is expressed as a set of equations relating the old image positions (coordinates) to the new ones. These equations need to be restricted (rigid body, affine, etc.) in order to limit the possible deformations of the image. Linear transformation will translate, rotate, zoom and shear one image to match it with another and usually works fine for within subject registrations. Sometimes the differences are such that the linear transformation is not sufficient (e.g. between subjects registration), hence local deformations permitted by nonlinear methods lead to a better result.

To align the previously segmented brain masks to diffusion space, image registrations were performed in our study using FMRIB's Linear and Nonlinear Image Registration Tools (FLIRT and FNIRT) (Andersson et al., 2007; Jenkinson and Smith, 2001).

3. Objectives

Generally, the aim of our research was to examine molecular alterations of CNS diseases *in vivo* using quantitative MRI methods – like DWI and T2 relaxometry – and novel image processing algorithms such as segmentation, registration and mono- and bi-exponential data fitting supplemented by advanced statistical approaches.

Our first experiment targeted relapsing remitting MS patients and matched controls to characterize bi-exponential diffusion related signal changes in the NAWM areas. Unlike previous studies, this experiment provides deeper insights into the effects of age and lesion load on different water fractions.

Additionally, we wanted to shed additional light on WM diffusion changes with respect to epilepsy related diffusion parameters such as age at epilepsy onset (AAO) and chronic seizure activity. Therefore, we investigated diffusion changes in the WM of mesial-temporal lobe epilepsy patients with unilateral hippocampal sclerosis (MTLE-HS) and compared them to an age- and sex-matched control group. We hypothesized that chronic WM damage occurs in both the early and late onset disease groups, but the extent of that is different according to the timing of epilepsy onset.

Since the disc degeneration and the associated changes are believed to be crucial factors in low back pain, the development of a classification system based on quantitative assessment would help to detect the degeneration grade independently of human bias or errors. Thus, we planned to investigate the possible intra- and interobserver differences and to define quantitative T2 cut-off values with regard to two morphological classification systems – Pfirrmann and Schneiderman – in patients with intervertebral disc degeneration.

4. Materials and methods

4.1. Bi-exponential diffusion signal decay in normal appearing white matter of multiple sclerosis

4.1.1. Subjects

Fourteen MS patients (4 M/10 F; age range 22–50 years; mean age±SD 36.86±9.45 years) with supra- and infratentorial WM lesions were chosen according to McDonald criteria [30] from the Department of Neurology, University of Pécs. All the patients had relapsing-remitting subtype of MS. Physical disability was measured with expanded disability status scale (EDSS) by a clinical neurologist of the Department of Neurology, University of Pécs (Kurtzke, 1983). The measurements had taken place in the remission phase of the disease and 12 of the patients (86%) received chronic immunomodulatory or immunosupressive therapy of which 50% were on interferon beta-1a, 42% on interferon beta-1b and 8% on glatiramer acetate treatment. MR measurements were performed at least 3 months after the last relapse or steroid treatment. Patients with history of alcohol or drug abuse, psychiatric illness, traumatic brain injury, neurological disease (other than MS) were excluded from the study.

The age- and sex-matched control group (N=14, 4 M/ 10F; age range 19–51 years; mean age±SD 36.93±9.59 years) were requested to fill out a self-administered questionnaire immediately before the MRI examination. The questions were designed to focus on general health information, including neurological and psychiatric disorders, headache, hypertension, diabetes, medication, previous traumatic brain injury and environmental exposures such as alcohol and drugs. Control volunteers were excluded if they had abuse of alcohol or drugs, psychiatric illness, traumatic brain injury or a history of significant medical or neurological conditions that would be associated with remarkable changes in the brain such as diabetes, seizures, stroke, transient ischemic attack or migraine headache. For the evaluation of changes in diffusion, all participants (14 controls and 14 MS patients) were separately dichotomized into two subgroups based on the median age of 36 years as younger groups (N=7, 2 M/5F controls and N=7, 2 M/5F MS patients) and older groups (N=7, 2 M/5F controls and N=7, 2 M/5F MS patients). The average age of younger controls (29.00 ± 5.92; range: 19–36 years) and MS patients (28.86 ± 4.71; range: 22–35 years) or older controls (44.86 ± 4.18; range: 38–51 years) and MS patients (44.86 ± 4.67;

range: 37–50 years) did not differ significantly. Table 1 shows the clinical datasets for MS patients dichotomized into two subgroups.

The experimental protocol was approved by the ethical committee of the University of Pécs, and every participant gave and signed their informed consent prior to the examinations.

Table 1. Clinical characteristics of multiple sclerosis patients

Clinical variables	All patients (N=14)	Younger group (<36 years)	Older group (>36 years)	*p* value†
TLV (mL)	11.22 ± 13.10 (0.35-48.63)	16.82 ± 16.07 (2.9-48.6)	5.62 ± 6.33 (0.35-19.30)	ns**
TLN	26.07 ± 19.08 (2-63)	34.57 ± 20.86 (7-63)	17.57 ± 13.61 (2-40)	ns
EDSS	1.64 ± 1.57 (0.0-4.0)	1.14 ± 1.24 (0.0-3.5)	2.14 ± 1.80 (0.0-4.0)	ns
DD (years)	2.86 ± 3.45 (0.0-12.5)	2.50 ± 4.47 (0.0-12.5)	3.21 ± 2.34 (1.5-7.5)	ns**
Last relapse before MRI (months)	12.43 ± 13.02 (3.0-48.0)	5.43 ± 3.51 (3.0-11.0)	19.43 ± 15.52 (3.0-48.0)	ns**
Relapses before MRI	3.86 ± 2.88 (1.0-12.0)	4.29 ± 3.68 (2.0-12.0)	3.43 ± 2.0 (1.0-7.0)	ns**

TLV, total lesion volume; TLN, total lesion number; EDSS, Expanded Disability Status Scale; DD, disease duration; MRI magnetic resonance imaging
Values given as: mean ± standard deviation (range)
†t-test of differences in clinical variables between younger and older groups of MS
**Mann-Whitney U test

4.1.2. Magnetic resonance imaging

The measurements were carried out using a 3T Magnetom TIM Trio whole-body MRI scanner (Siemens AG, Erlangen, Germany) with a 12-channel phased array head coil. Beyond the routine T1-, T2- and diffusion-weighted measurements, fluid attenuated inversion recovery (FLAIR) imaging was also performed. 2D FLAIR images were acquired with a turbo spin echo sequence: TR/TI/TE=12400/2600/98 ms, 100 axial slices, slice thickness=1.1 mm, distance factor=0% (i.e. no gap), interleaved slice order with 2 concatenation, field of view (FOV)=211×211 mm^2, matrix size=192×192, bandwidth=286 Hz/pixel, turbo-factor=14. To investigate the bi-exponential diffusion signal decay, a diffusion-weighted 2D spin-echo echo-planar imaging (EPI) sequence using a 3-scan trace mode was performed with the following parameters: TR/TE=4800/128 ms, 20 axial slices, slice thickness=3.5 mm, interslice gap=1.0 mm, FOV=188×250 mm^2, matrix size=144 × 192, bandwidth=1302 Hz/pixel, number of averages=5, b-values=0, 500, 1000, 2000, 3000, 4000, 5000 s/mm^2. Diffusion weighting was applied in the (1.0 1.0 -0.5), (1.0 -0.5 1.0) and (−0.5 1.0 1.0) directions, where these are vectors along the physical XYZ axes directions. Trace image was formed for each b-value (except b=0 s/mm^2) by calculating the geometric mean (I) of the signals in the three orthogonal spatial directions (see E.q. 4).

4.1.3. Data analysis

Lesion load and normal appearing white matter analysis

WM lesions were considered if visible (as being hyperintense) on T2-weighted and FLAIR images and the extent was larger than 3 mm (Vermeer et al., 2003). A neurologist with a clinical and imaging experience in MS, blinded to clinical and neuropsychiatric findings performed the lesion load assessments in the Department of Neurology, University of Pécs. Lesions were outlined manually on FLAIR images using the semi-automated thresholding technique in 3D-Slicer software (http://www.slicer.org, Version 3.6.3). The method relied on user-guided specification of the intensity threshold range, which was manually adjustable during lesion segmentation. The algorithm labels all pixels within the applied threshold range in the lesion area identified manually by the user. The volumes of label maps were estimated using 3D-Slicer's Label Statistics module. WM lesions were counted and volumes were measured (in mL) for each patient. The calculated results were categorized as

total lesion volume (TLV) and total lesion number (TLN) from the bilateral frontal, parietal, temporal and occipital lobes which were used for further calculations. NAWM was defined as an area with normal signal intensity on T1-, T2-weighted and FLAIR images.

ROI measurements

The free-hand regions of interest (ROIs) were drawn bilaterally and symmetrically on images acquired without diffusion weighting gradients (b=0 s/mm^2) by referring to FLAIR images. ROIs of 19–52 pixels (mean volume: 218.81±44.61 mm^3 range: 112–308 mm^3) were placed in the pre-defined normal appearing frontal, occipital and centrum semiovale areas of MS patients and controls, where the ROI size did not differ significantly. The ROIs of NAWM areas were sampled on a given slice of the image series in both control and MS patient groups to avoid possible partial volume effects. The selected regions were strictly defined anatomically and partial volume effects minimized by inspecting the slices above and below the region in order to avoid averaging with lesions, GM or cerebrospinal fluid. The frontal NAWM was sampled, where the frontal horns of the lateral ventricles in both hemispheres were visible, the occipital lobe ROIs were placed, where the left and right occipital horn of the lateral ventricles were clearly defined and ROIs for centrum semiovale were placed on an axial slice above the bilateral ventricles (Figure 10). All NAWM ROIs were obtained and the diffusion analyses were made by a single observer (S.A.N., MRI radiographer) blinded to the clinical details.

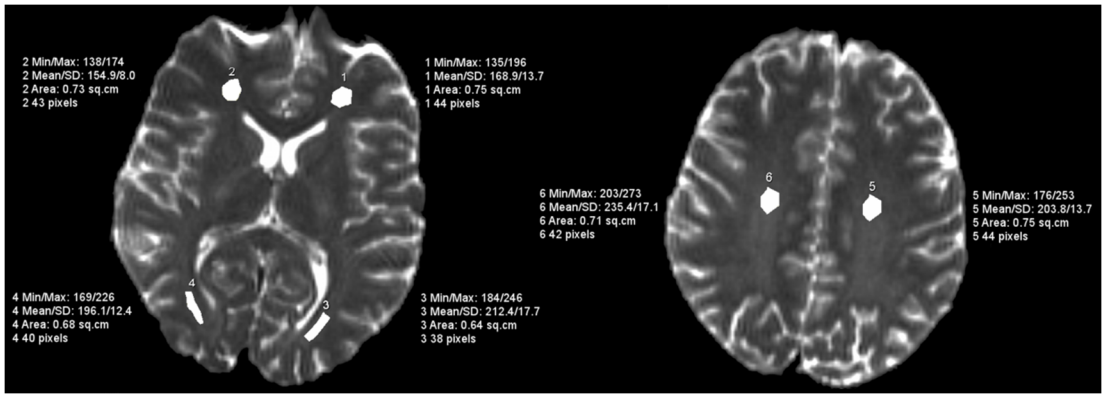

Figure 10. Bilateral regions of interest localisations of diffusion measurements: 1-2: Frontal WM; 3-4: Occipital WM; 5-6 Centrum semiovale.

Diffusion analysis

Diffusion data processing was carried out using Matlab® software's curve fitting toolbox and a self-written program code (The MathWorks, Inc., Natick, MA). Apparent diffusion coefficient was measured within each ROI by calculating and mono-exponentially fitting the mean signal intensity for the b0, b500 and b1000 images using E.q. 4.

The ADC value of each ROI was broken into ADC_{fast} and ADC_{slow} by applying a bi-exponential fit (E.q. 5) throughout the whole b-value range (b0-b5000). Henceforth, ADC_{fast}, ADC_{slow} and f_{slow} are noted as ADC_f, ADC_s and f_s respectively in the thesis. The mean ADC, ADC_f, ADC_s, f_s values of NAWM were calculated from ROI-pairs separately as frontal, occipital WM and centrum semiovale (Figure 10) and averaged as total NAWM. All diagrams in the paper show the mean raw data (uncorrected) of total NAWM diffusion.

Statistical analysis

Data analysis was performed using SPSS statistical software, version 19.0 (SPSS, Inc., Chicago, IL). All measured parameters and clinical data are presented as mean±standard deviation. Normality of data distribution was tested by Shapiro-Wilk statistics. Homogeneity of variance was shown by Levene's test. Differences were established by two-tailed t-tests for Gaussian values with Welch's correction for unequal variances, and Mann–Whitney U tests for non-Gaussian distributions. Pearson or Spearman correlation tests were used to determine the strength of the relationship between two continuous variables. A two-tailed level of $p \leq 0.05$ was the significance threshold for all statistical analysis. In addition, multiple linear regression model was used to assess the relationship of NAWM diffusivity to age and gender in control group, while it was used to determine whether NAWM diffusion (dependent variable) was related to such predictors as age, gender, TLV, TLN, EDSS or disease duration (DD) in patient group. Predictors were introduced in a forward stepwise manner and retained in the model only if $p<0.05$ was achieved. The assumptions of multiple linear regressions were satisfied, as judged by testing for linearity, normality assumptions of the residues, outliers, independence of errors, homoscedasticity and multi-collinearity (Chan, 2004).

4.2. Age at onset and seizure frequency affect white matter diffusion coefficient in patients with mesial-temporal lobe epilepsy

4.2.1. Subjects

Inclusion criteria for patients were the following:

(1) detailed presurgical evaluation or under the care of an outpatient clinic;

(2) head MRI with epilepsy-specific protocol; and

(3) unilateral hippocampal sclerosis.

Twenty-two patients (14 females) with temporal lobe epilepsy accompanied by unilateral hippocampal sclerosis were enrolled in the study (14 right-sided, 8 left-sided). All patients in the study presented initially to the tertiary epilepsy centre and underwent 32- to 64-channel surface noninvasive electroencephalogram (EEG) monitoring. The electrodes were placed according to the 10–10 system. The number of electrodes and their placement varied individually corresponding to the suspected epileptogenic region and side but FP1, F3, C3, P3, O1, F7, FT7, T7, TP7, P7,108 FT9, TP9, homologous right-sided electrodes, PZ, CZ, FZ were always used. Thirteen patients underwent an adult presurgical evaluation protocol including continuous video-EEG monitoring, neuropsychological testing, and high-resolution head MRI with epilepsy-specific protocol. The remaining nine patients were examined with long-term EEG, and they also had high-resolution head MRI with epilepsy-specific protocol. Clinical MR images were analysed by a trained neuroradiologist with 23 years of experience in epilepsy imaging. Neither high resolution head MRI with epilepsy-specific protocol nor presurgical evaluation using continuous video-EEG monitoring showed the existence of bitemporal epilepsy. Patients with neurodegenerative disorders, intracranial tumours, and cognitive deficits and those who underwent previous brain surgery were excluded from the study. The following clinical data were collected for each patient with MTLE-HS before the MRI examination: age, sex, seizure frequency, AAO, DD, level of education, history of febrile seizure, occurrence of generalized tonic-clonic seizure within the last 5 years, current and previous antiepileptic drugs, head trauma prior to AAO, history of brain infections such as encephalitis/meningitis, and possible perinatal complication.

Seizure frequency was determined from the seizure diary completed by the patient and defined as the mean frequency of complex partial seizures per month during at least the last 12 months prior to enrolment. In order to examine the effect of AAO on WM diffusion, patients were divided into two groups according to the median AAO: one group of patients with early onset MTLE-HS (N=11; 9 females) with AAO≤16 years and the other group of subjects with late onset MTLE-HS (N=11; 5 females) with AAO>16 years. All patients were taking antiepileptic medication at the time of study. Six patients (1 patient with early onset MTLE-HS) were treated with a single drug (carbamazepine [CBZ], levetiracetam [LEV], oxcarbazepine [OXCBZ], or valproate [VPA], whereas sixteen patients (10 patients with early onset MTLE-HS) received more than one drug. Lamotrigine (LTG) and clobazam were used most frequently as adjunct drugs in these cases. Carbamazepine/OXCBZ or sodium channel blockers (LTG, CBZ, OXCBZ, and lacosamide) as a group or drug polytherapy showed no significant effect on diffusion in the ipsilateral hemispheric and temporal lobe WM or in the uncinate fasciculus. Therefore, these variables were not considered as confounding factors in the final statistical models. Clinical and demographic details for patients with MTLE-HS are summarized in Table 2.

Table 2. Clinical and demographic details for MTLE-HS patients.

Investigated data	MTLE-HS patients		
	Early onset group (N=11)	***Late onset group (N=11)***	***Total (N=22)***
age (years)[a]	39.3±13.8 (19-61)	47.4±13.7 (20-63)	43.3±14.1 (19-63)
seizure frequency[a, ‡]	4.7±5.4 (0-20)	3.2±5.3 (0-18)	4.0±5.2 (0-20)
AAO (years)[a]	7.6±5.5 (1-16)	38.3±13.5 (17-57)	23.0±18.6 (1-57)
level of education (years)[a]	12.7±3.5 (8-17)	11.8±2.9 (8-16)	12.3±3.1 (8-17)
history of febrile seizure	5	2	7
occurrence of GTCS	3	5	8
head trauma prior to AAO	0	2	2
mild encephalitis/meningitis	3	0	3
perinatal complication	1	0	1

MTLE-HS: Mesial-temporal lobe epilepsy with hippocampal sclerosis; AAO: age at epilepsy onset; GTCS: generalized tonic-clonic seizure within the last 5 years.

[a] Values given as: mean ± standard deviation (range).

‡ Seizure frequency was defined as the mean frequency of complex partial seizures per month during at least the last 12 months prior to enrolment.

Twenty-two healthy control subjects (14 females; age range: 19–66 years; mean age: 43.5±14.4 years) were also examined and matched for age and sex to the patient group with early onset MTLE-HS (N=11, 9 females; age range: 19–56 years; mean age: 39.4±13.9 years) and the patient group with late onset MTLE-HS (N=11, 5 females; age range: 21–66 years; mean age: 47.6±14.2 years). Control volunteers were not included if they had a history of alcohol or drug abuse, psychiatric illness, traumatic brain injury, or history of significant medical or neurological conditions that would be associated with remarkable changes in the brain such as seizures, stroke, or migraine headache.

4.2.2. Magnetic resonance imaging

All the measurements were carried out using a 3T Magnetom TIM Trio whole-body MRI scanner (Siemens AG, Erlangen, Germany). In all patients, at least two MRI examinations were performed: a) An MRI with epilepsy-specific protocol which is part of our standard clinical practice and which also screened for HS as an inclusion criterion for this study. Beyond the routine axial, coronal T2- weighted measurements, the epilepsy-specific protocol also contained the 2D FLAIR imaging sequence with fat suppression and T1-weighted high-resolution images (voxel size: 0.98×0.98×0.98) to detect subtle structural alterations in the mesial temporal lobe. Routine DWI was carried out to localize the epileptogenic foci. b) An MRI with research protocol was also obtained for all patients between January 2013 and June 2015 at least 48 h after the last ictus. For tissue segmentation and registration, a T1-weighted 3D magnetization-prepared rapid acquisition with gradient echo (MPRAGE) sequence was utilized using the following parameters: TR/TE/TI=2530/3.4/1100 ms; flip angle=7°; 176 sagittal slices; slice thickness=1 mm; FOV=256×256 mm^2; matrix size=256×256; bandwidth=200 Hz/pixel. To investigate diffusion signal changes, a diffusion-weighted 2D spin-echo EPI sequence using a 3-scan trace mode was performed (TR/TE=4800/128 ms; slice thickness=3.5 mm; interslice gap=1 mm; FOV=188×250 mm^2; matrix size=144×192; bandwidth=1302 Hz/pixel; number of averages=5; b-values=0, 500, 1000 s/mm^2). Diffusion weighting was applied in the (1.0 1.0 −0.5), (1.0 −0.5 1.0), and (−0.5 1.0 1.0) directions. Trace image was formed for each b-value (except b=0 s/mm^2) by calculating the geometric mean (*I*) of the signals in the three orthogonal spatial directions (see E.q. 4).

4.2.3. Data analysis

Pre-processing

Diffusion data were first corrected for eddy current distortion and simple head motion using a 12-degrees-of-freedom affine registration to the volume without diffusion-weighting (Rohde et al., 2004). The Brain Extraction Tool, provided by FMRIB Software Library, was applied on both MPRAGE and DWI data to eliminate nonbrain tissues (Smith, 2002).

Regions of interest analysis

Subcortical hemispheric WM was segmented by FAST to evaluate global WM deviations (Zhang et al., 2001). In order to examine regional subcortical WM abnormalities, frontal, temporal, parietal, and occipital WM lobes were segmented using Freesurfer 5.3 image analysis suite (https://surfer.nmr.mgh.harvard.edu/) (Fischl et al., 2002). Error correction was performed when necessary, based on the recommended reconstruction workflow (https://surfer.nmr.mgh.harvard.edu/fswiki/RecommendedReconstruction). To evaluate diffusion changes in specific WM bundles, three regions of the limbic tracts (left and right hippocampal cingulum, fornix cres with stria terminalis, uncinate fasciculus) and one region of association tract (left and right sagittal stratum including inferior longitudinal fasciculus and inferior fronto occipital fasciculus) were created as ROIs using ICBM-DTI-WM atlas with reference to the MRI (Oishi et al., 2010). These regions were chosen because they present the location where functional abnormalities have been consistently observed in patients with MTLE-HS (Ahmadi et al., 2009; Diehl et al., 2008). Image registrations were performed using FLIRT and FNIRT (Andersson et al., 2007; Jenkinson and Smith, 2001). For tract-based analysis, MPRAGE images were spatially registered into MNI152 T1-weighted 1-mm standard space image using a two-step process: 1) brain-extracted MPRAGE was linearly registered to standard space with 12-degrees-of-freedom, and 2) after registration was refined by FNIRT, an inverse transformation was applied to warp the ICBM-DTI-WM atlas labels into the MPRAGE space. In order to derive WM labels, the brain-extracted b0 image of each subject was linearly registered to that subject's brain-extracted MPRAGE image using a 6-degrees-of-freedom linear fit. Finally, the inverse of the spatial transformation from diffusion space to MPRAGE space was applied to align the segmented brain masks to diffusion space, where diffusion analyses were

performed. The resulting masks were eroded by using a 2D kernel of 3×3×1 voxels to avoid partial volume effects and to minimize possible impacts of misregistration. Regions of interest were defined as the eroded WM masks and obtained separately for both left and right sides of the structures (Figure 11).

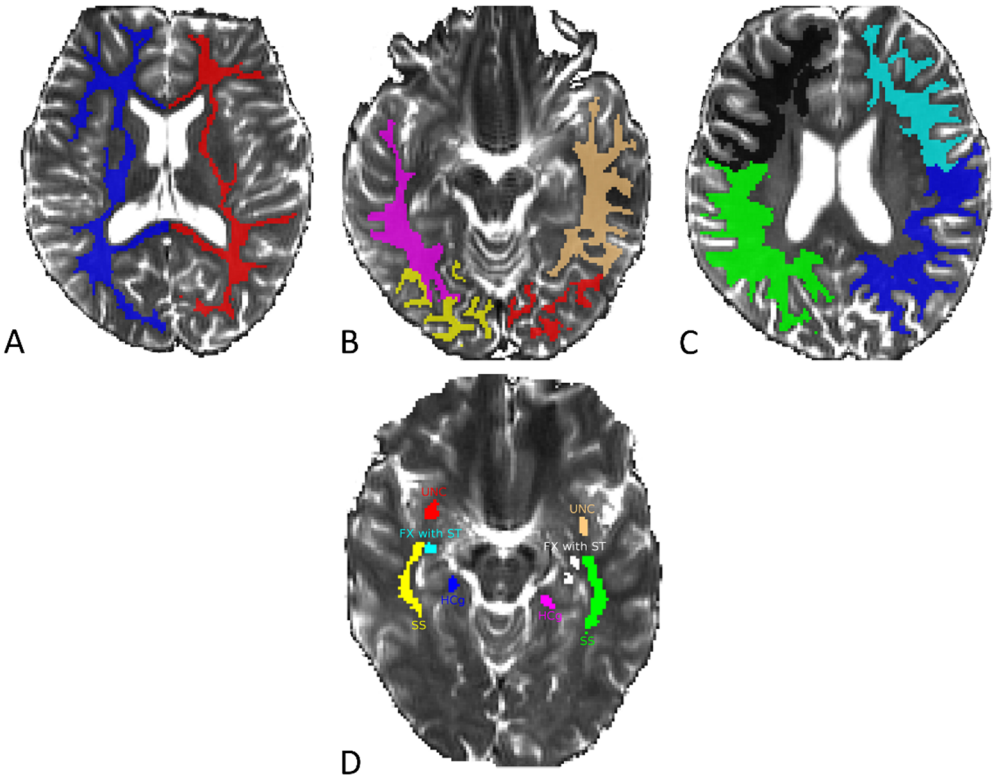

Figure 11. Representations of the regions of interest analysis. Regional averages of ADC values were extracted from diffusion-weighted images using eroded masks of the left and right hemispheric WM (A); temporal, occipital lobes WM (B); frontal, parietal lobes WM (C); Uncinate Fasciculus (UNC); Fornix cres with Stria terminalis (FX with ST); Hippocampal Cingulum (HCg); Sagittal Stratum (SS) include inferior longitudinal fasciculus and inferior fronto-occipital fasciculus (D). Images are presented in radiological convention.

Diffusion analysis

Diffusion data processing was carried out using Matlab® software's curve fitting toolbox and a self-written program code (The MathWorks, Inc., Natick, MA). Apparent diffusion coefficient was measured within each ROI by calculating and mono-exponentially fitting the mean signal intensity for the b0, b500, and b1000 images using the equation of E.q. 4.

Statistical analysis

Data analyses were performed using SPSS® statistical software version 20.0 (IBM Corp., Armonk, NY). Differences were estimated by independent two-tailed t-tests for Gaussian values. Before using parametric t-tests, the homogeneity of variance was inspected by Levene's test, while the normality of data was examined by Shapiro–Wilk statistics for independent samples. Welch's correction was applied for parametric data demonstrating unequal variances. Multiple linear regression models were constructed to determine whether ADC was related to AAO, seizure frequency, age, sex in patients and to age and sex in the control group. The assumptions of multiple linear regressions were satisfied, as judged by testing for linearity, normality assumptions of the residues, outliers, independence of errors, homoscedasticity, and multi-collinearity (Chan, 2004). Results were considered significant at $p \leq 0.05$ for all statistical tests.

4.3. A Statistical Model for Intervertebral Disc Degeneration: Determination of the Optimal T2 Cut-Off Values

4.3.1. Subjects

Twenty-one patients (13 females, 8 males; age range: 14–80 years; mean age 51.14±18.88 years) with single or recurrent episode of low back pain were examined. All the patients in this study presented initially to the outpatient spine clinic and then were referred for a lumbar MRI. Exclusion criteria were contraindication for MRI, previous malignant disease or injury in the lumbar spine. No patients had evidence of lumbar disorders except IVDD or herniation. The experimental protocol was approved by the local Ethical Committee and performed in accordance with the ethical standards described in the Declaration of Helsinki (1964). Every participant was informed about the procedure and signed their informed consent prior to the examination.

4.3.2. Magnetic resonance imaging

The measurements were carried out using a 3T Magnetom TIM Trio whole-body MRI scanner (Siemens AG, Erlangen, Germany) using a dedicated eight-channel spine coil (3T Spine matrix Coil, Siemens AG, Erlangen, Germany). Both morphological and quantitative MRI was performed covering the intervertebral discs L1-L2 to L5-S1. Beyond the conventional sagittal, axial T2- and T1-weighted measurements, T2 relaxometry was also performed. Quantitative multi-echo T2 imaging was carried out using a CPMG imaging sequence in the sagittal section with the following parameters:

TR=2370 ms; 20 equally spaced echoes between 10 and 200 ms; slice thickness=6 mm; interslice gap=1 mm; FOV=256×256 mm^2; matrix=256×256; bandwidth=186 Hz/px; number of averages=1. All the imaging sequences were acquired without fat suppression.

4.3.3. Data analysis

Morphological evaluation

All discs were classified morphologically according to the Pfirrmann and Schneiderman classification systems on sagittal T2W turbo spin echo images by three neuroradiologists with 9, 10, and 12 years of experience in MR image analysis of the spine, respectively. The three neuroradiologists blindly classified the grade of disc degeneration as grade I–V in the midsagittal section according to the Pfirrmann classification (Pfirrmann et al., 2001) [4], while the Schneiderman scheme was classified as grade 0–3 depending on the degeneration level (Grade 0: normal height and signal intensity; Grade 1: speckled pattern or heterogeneous decreased intensity; Grade 2: diffuse loss of signal; and Grade 3: signal void) (Schneiderman et al., 1987). The morphological classification of disc degeneration was assessed independently; therefore differences were not settled by consensus. For intraobserver reliability analysis, three experienced observers analysed all scans twice, with an interval of 5 months, and intraobserver differences between the separate occasions were calculated thereafter. Interobserver reliability was measured between only the first readings of all observers.

Quantitative assessment

For T2 measurements, ROIs were manually drawn on a pre-selected echo (TE=130 ms) over the inner portion of the lumbar disc to cover the NP. To minimize the errors, all measurements were performed by a single investigator and the ROIs were sampled on a given slice of the midsagittal section of the NP to avoid possible partial volume effects (Figure 12). T2 relaxation time data processing was carried out in each ROI by one of the authors (S.A.N.) with the non-negative least squares algorithm using Matlab® software's curve fitting toolbox and a self-written program code (The MathWorks, Inc., Natick, MA). For T2 measurements, the odd echoes were excluded to minimize the error from stimulated echoes (Maier et al., 2003). The signal at each remaining point was measured and plotted as a function of time on a semi-log scale

where no curvature was found; therefore T2 relaxation time was measured by mono-exponentially fitting the mean signal intensity using equation E.q. 6.

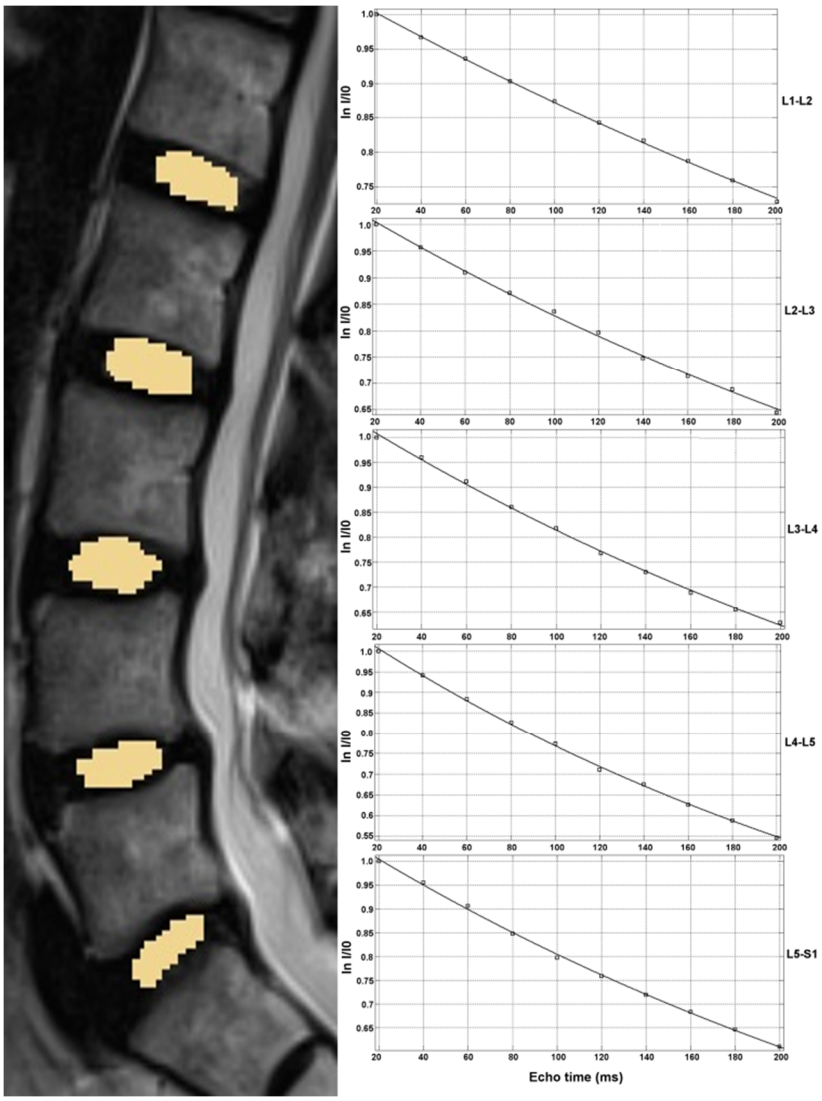

Figure 12. Regions of interest placement of the lumbar discs with the corresponding normalized semi-log plots of signal versus echo time.

Statistical analysis

Data analysis was performed using SPSS statistical software ® version 19.0 (SPSS, Inc., Chicago, IL). Multiple linear regression model was used to determine whether IVDD and T2 values were related to such predictors as age, gender, herniation and previous low back surgery. Predictors were introduced in a forward stepwise manner and retained in the model only if $p \leq 0.05$ was achieved as determined with the F-test. The assumptions of multiple linear regressions were satisfied, as judged by testing for linearity, normality assumptions of the residues, outliers, independence of errors, homoscedasticity, and multi-collinearity (Chan, 2004). To test intraobserver

reliability Cohen's Kappa analysis was used by the bootstrap method with 1,000 replications, while interobserver agreement among multiple observers was calculated according to generalized Kappa statistics based on the standard least square approach (Landis and Koch, 1977). Chi-square analysis was performed to determine whether the observed counts significantly differ from the expected distribution. In addition, receiver operating characteristic analysis was performed among grades to determine the T2 cut-off values in each classification. Kappa statistics were interpreted as follows: values between 0 and 0.2 indicate slight agreement, 0.21–0.4 indicates fair agreement, 0.41–0.6 indicates moderate agreement, 0.61–0.8 indicates substantial agreement and >0.81 indicates almost perfect agreement (Viera and Garrett, 2005). The level of $p \leq 0.05$ was the significance threshold for all statistical analysis.

5. Results

5.1. Bi-exponential diffusion signal decay in normal appearing white matter of multiple sclerosis

5.1.1. MS lesions volume

The mean TLN was 26.07±19.08 and the mean TLV was 11.22±13.10 mL. Both the mean TLN and TLV were higher in the younger group compared with the older MS group (Table 1). Frontal lesions represented the greatest percentage of TLN (55.07%) and TLV (34.35%). Regional and total lesion numbers or volumes were correlated; in case of lesion number, frontal and parietal areas showed the highest correlation with TLN ($p<0.0001$; Pearson $r=0.94$ and 0.95, respectively); while lesion volumes of temporal and frontal areas robustly correlated with TLV ($p<0.0001$; Spearman $r=0.93$ and 0.84 respectively). There was a strong positive association between the TLN and TLV ($p=0.008$; Spearman $r=0.67$).

5.1.2. Significance of the investigated predictors

The stepwise multiple linear regression analyses revealed that the NAWM diffusivity of MS patients was significantly related to age ($p=0.03$) and TLN ($p=0.04$), but no significant association with TLV, EDSS and DD was found. There was no effect of gender in either control or patient groups. These independent parameters were not considered as confounding factors in later statistical models.

5.1.3. Mono- and bi-exponential analysis of NAWM diffusivity

In controls, ADC slightly increased with age in NAWM areas (bilateral frontal and occipital WM; centrum semiovale) as well as total NAWM (Figure 13); however the difference between the younger and older age groups was not significant.

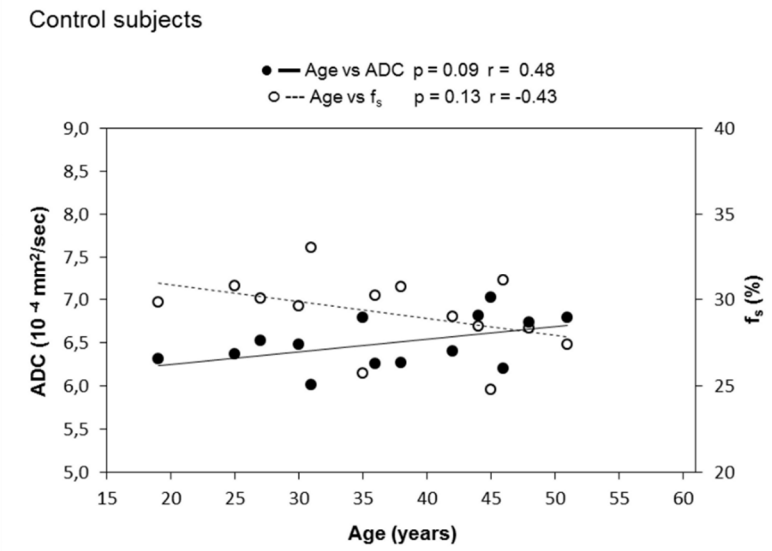

Figure 13. The figure illustrates the age-dependent changes of ADC (●─ p=0.09 r=0.48) and f_s values (○---p=0.13 r=-0.43) in control subjects.

ADC, apparent diffusion coefficient; f_s, volume fraction of slow diffusing component

In MS patients, linear regression analysis showed a decreasing trend of TLN with increase of age (p=0.21 r=−0.36); however ADC values of NAWM inversely related to age and depend linearly on TLN (Figure 14 and 15).

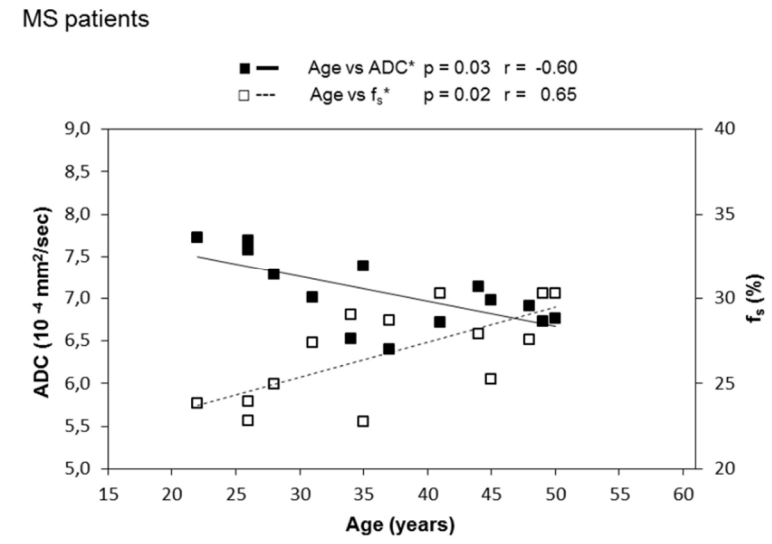

Figure 14. The diagram shows a significant negative relationship of ADC with age in MS patients (p=0.03), nevertheless the unfilled square markers depict a notable age-dependent increase of f_s (p=0.02). In case of young MS patients having elevated lesion number ADC values are higher, while f_s values are lower compared with older patients.

*Adjusted for total lesion number.

ADC, apparent diffusion coefficient; MS, multiple sclerosis; f_s, volume fraction of slow diffusing component

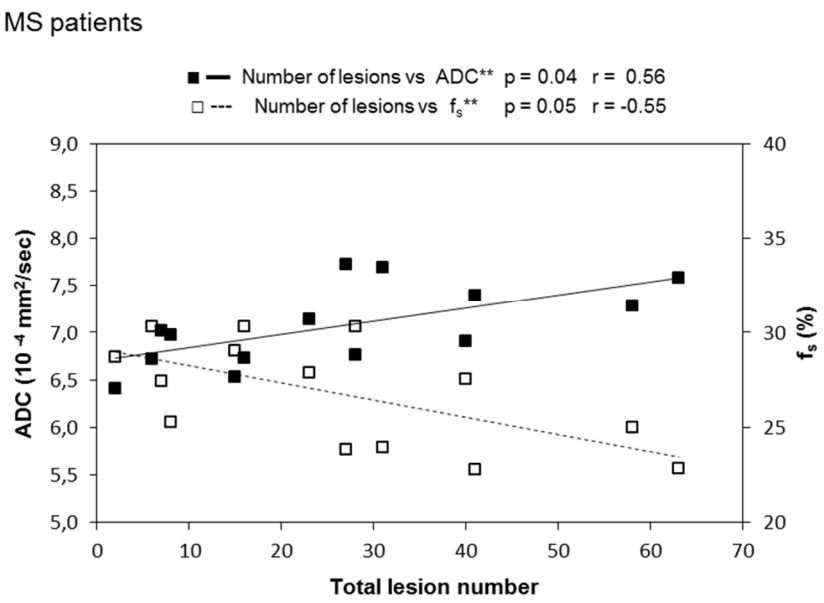

Figure 15. The figure depicts the relationship between total lesion number and diffusion measurements of both ADC and f_s in MS patients. ADC significantly increases (p=0.04) while f_s decreases (p=0.05) with total lesion number causing higher ADC values, but lower f_s in patients with elevated lesion number.

**Adjusted for age.

ADC, apparent diffusion coefficient; MS, multiple sclerosis; f_s, volume fraction of slow diffusing component

Centrum semiovale showed the strongest negative relationship of ADC against age adjusted for TLN (p=0.007 r=−0.49, not shown), while only the ADC of total NAWM depicted significantly positive relation as a function of TLN. ADC was robustly different between controls and MS patients when considering all participants or younger groups; however in older groups the ADC was similar and no significant differences were found in NAWM (Table 3).

Table 3. Comparison between diffusion measurements of MS patients and control subjects in all participants, younger and older groups

Groups	Localisation	*p* values of MS patients vs. controls			
		ADC	ADC_f	ADC_s	f_s
All participants	Frontal WM	<0.05	ns**	ns	0.08
	Occipital WM	<0.01	ns	ns*	ns
	Centrum semiovale	<0.001	<0.01	ns	<0.05
	Total NAWM	**<0.001**	**<0.05**	**ns***	**<0.05**
Younger	Frontal WM	<0.01	ns	ns**	0.06
	Occipital WM	<0.05	ns	ns	<0.05**
	Centrum semiovale	<0.001	<0.001	ns	<0.001
	Total NAWM	**<0.001**	**0.05**	**ns***	**<0.01**
Older	Frontal WM	ns	ns	ns	ns
	Occipital WM	ns	ns	ns*	ns
	Centrum semiovale	ns	ns	ns*	ns
	Total NAWM	**ns**	**ns**	**ns***	**ns**

WM, white matter; NAWM, normal appearing white matter; MS, multiple sclerosis; ADC, apparent diffusion coefficient; ADC_f and ADC_s, fast and slow diffusing component; f_s, volume fraction of slow diffusing component
*Welch correction
**Mann-Whitney U test

The results of bi-exponential analyses of NAWM are listed in Table 3 and 4. Significant inverse correlations were found between ADC and f_s in both controls and MS patients. However, there was no association between ADC and ADC_s or ADC_f in any of the examined NAWM using Pearson correlations (data not shown). ADC_f and ADC_s did not change as a function of either age in controls or lesion number and age in MS patients. Figure 13 shows a decreasing trend of f_s with age in controls, but the difference between the two age groups was not significant. In MS patients, f_s increased as a function of age and decreased with TLN in NAWM. These relations were significant in total NAWM (Figure 14 and 15). In case of regional analysis, only centrum semiovale depicted a significant positive relation of f_s with age ($p=0.003$ $r=0.75$ adjusted for TLN; not shown), while only frontal WM represented an inverse significant relationship of f_s as a function TLN ($p=0.04$ $r=-0.57$ adjusted for age; not shown). In MS patients, f_s was significantly different between younger and older groups in total NAWM and centrum semiovale (Table 4), moreover younger controls and MS patients showed the most significant difference in the same areas (Table 3).

Table 4. Mean diffusion measurements ± SD (10^{-4} mm^2/s) and *p* values of NAEM in multiple sclerosis patients

Localisation	Groups	ADC	*p* value (ADC)	ADC_f	*p* value (ADC_f)	ADC_s	*p* value (ADC_s)	f_s (%)	*p* value (f_s)
Frontal WM	younger	7.20 ± 0.51	<0.05	12.71 ± 0.42	ns	0.78 ± 0.13	ns	25.60 ± 3.88	ns
	older	6.58 ± 0.39		12.43 ± 0.51		0.79 ± 0.13		28.18 ± 2.53	
Occipital WM	younger	7.54 ± 0.62	ns	12.28 ± 1.15	ns**	0.84 ± 0.22	ns	23.34 ± 2.18	ns
	older	7.25 ± 0.48		12.50 ± 0.50		1.08 ± 0.33		26.54 ± 3.64	
Centrum semiovale	younger	7.21 ± 0.47	<0.01	12.61 ± 0.36	ns	0.98 ± 0.13	ns*	25.96 ± 2.76	<0.01
	older	6.60 ± 0.28		12.60 ± 0.86		1.19 ± 0.33		31.10 ± 3.36	
Total NAWM	younger	7.31 ± 0.43	**<0.05**	12.54 ± 0.36	**ns**	0.87 ± 0.12	**ns***	24.97 ± 2.38	**<0.01**
	older	6.80 ± 0.23		12.50 ± 0.39		1.02 ± 0.21		28.61 ± 1.89	

SD, standard deviation; WM, white matter; NAWM, normal appearing white matter; ADC apparent diffusion coefficient; ADC_f and ADC_s, fast and slow diffusing component; f_s, volume fraction of slow diffusing component

*Welch correction

**Mann-Whitney U test

Accuracy of the bi-exponential parameters considerably depends on the noise level, however the SNR was large enough even on the images acquired with high b-values. Figure 16 shows representative diffusion maps (a) and mean SNR values (b) for both the MS and control groups.

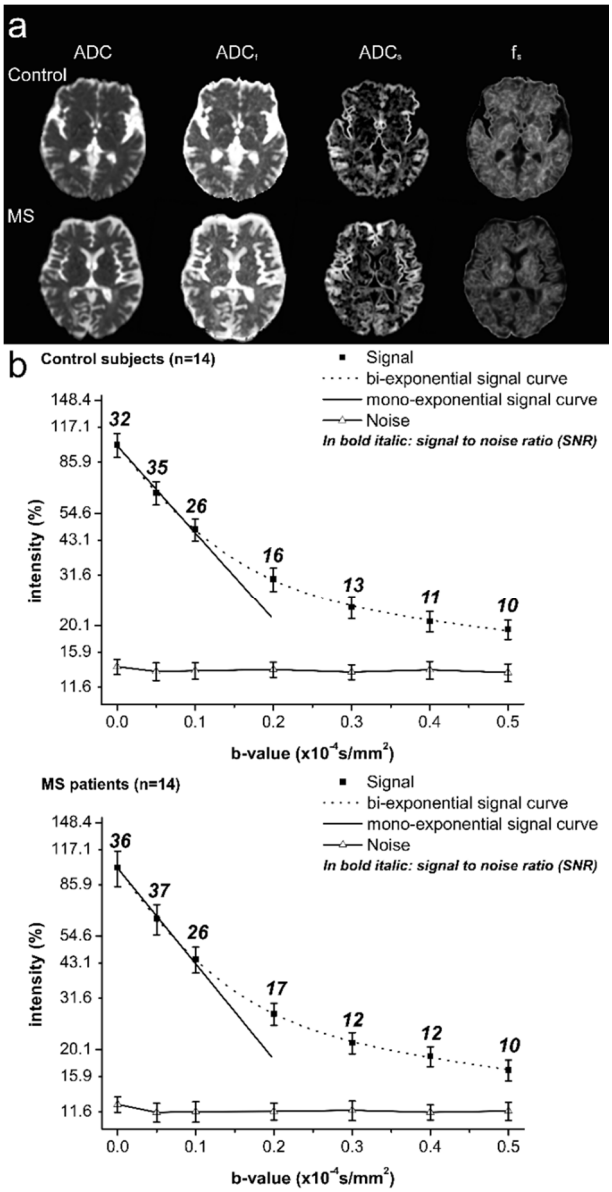

Figure 16a shows the diffusion maps of a representative normal control and an MS patient. Figure 16b illustrates the average diffusion-weighted signal decay on logarithmic scale with bi-exponential and mono-exponential fits for the NAWM of the two examined groups. The SNR (i.e. average signal intensity over the standard deviation of the noise) is also demonstrated for each b-value. Intensity values with their standard deviations are shown in normalized units.

ADC, apparent diffusion coefficient; ADC_f and ADC_s, fast and slow diffusing component; f_s, volume fraction of slow diffusing component; MS, multiple sclerosis

5.2. Age at onset and seizure frequency affect white matter diffusion coefficient in patients with mesial-temporal lobe epilepsy

ADC values measured in patients were presented as the side ipsilateral and contralateral to the seizure focus and compared with the corresponding side of healthy controls.

5.2.1. Differences between groups

Except for the ipsilateral hemispheric and temporal lobe WM and the uncinate fasciculus, none of the other regions showed ADC difference between patients and controls. There was a significant ADC difference of the ipsilateral hemispheric WM between the whole patient and the control groups (Figure 17A). Here, patients in the group with early onset MTLE-HS showed higher ADC compared with their matched controls, but it disappeared in the group with late onset MTLE-HS (Table 5). In the ipsilateral temporal lobe WM, ADC was only borderline higher (p=0.056) in the whole patient group compared with controls (Figure 17B).

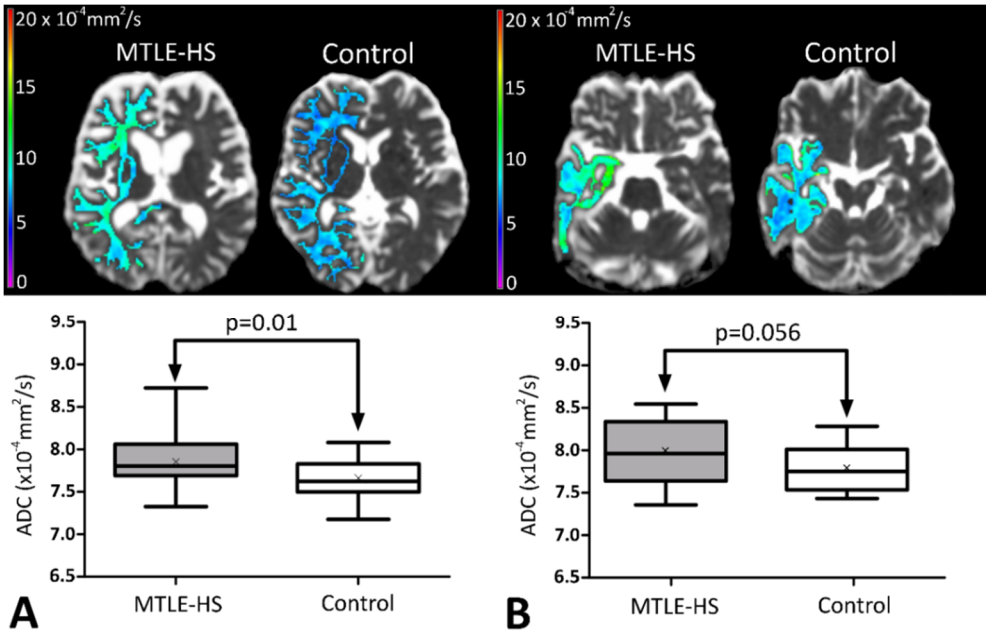

Figure 17 shows DWI images overlaid with color-coded ipsilateral hemispheric (upper left of A) and temporal lobe WM (upper right of B) ADC values in a representative MTLE-HS patient and a control subject. The box- and whiskers plots show the distribution of ADC values in the ipsilateral hemispheric (lower left of A) and temporal lobe WM (lower right of B) of MTLE-HS patients (N=22) and control subjects (N=22). The whiskers in the plot represent the minimum and the maximum ADC values, the cross depicts the mean while the band inside the box shows the median ADC.

MTLE-HS: Mesial-temporal lobe epilepsy with hippocampal sclerosis; ADC: Apparent diffusion coefficient.

Conversely, ADC was significantly elevated (p=0.01) in patients with early onset MTLE-HS (8.21±0.30) compared with controls (7.88±0.29), but this association was missing in patients with late onset MTLE-HS (Table 5). In the ipsilateral uncinate fasciculus, a significant ADC difference was observed (p=0.02) between the whole patient (7.93±0.50) and control groups (7.61±0.36); however, neither the patient group with early nor that with late onset MTLE-HS showed significant ADC elevation compared with controls (Table 5).

Table 5. Diffusion differences in the ipsilateral WM areas.

	Groups	Hemispheric WM	Temporal lobe WM	Uncinate fasciculus
MTLE-HS vs. Control	**Whole**	p=0.01	p=0.056	p=0.02
	Early onset	p=0.04	p=0.01	ns*
	Late onset	ns	ns	ns

MTLE-HS: Mesial-temporal lobe epilepsy with hippocampal sclerosis; WM: white matter; ns: not significant.
*Independent two-tailed t-test with Welch correction for unequal variances.

5.2.2. Differences within groups

Patients with early onset disease had higher ADC (p=0.04) in the ipsilateral side of temporal lobe WM (8.21±0.30) compared with that in the contralateral side (7.97±0.20), but this difference was not present in the group with late onset MTLE-HS. Besides the temporal lobe WM, data derived from patients were not significantly different between the ipsi- and the contralateral sides. Multiple linear regression analysis indicated significant effects of AAO, age, and seizure frequency on ADC, while no sex differences were observed in patients. There were no significant effects of either age or sex on ADC in controls. In the whole patient group, ADC showed negative relationship with AAO in the ipsilateral side of the hemispheric and temporal lobe WM and the uncinate fasciculus while ADC was positively related to age in the ipsilateral hemispheric WM and the uncinate fasciculus (corrected p and r values are in Table 6). In patients with early onset MTLE-HS, ADC was negatively related to AAO in the ipsilateral hemispheric WM (Table 6) and the uncinate fasciculus (Table 6, Figure 18A). In the ipsilateral temporal lobe WM, ADC tended to decrease as a function of AAO, but no significant correlation was found between them (Table 6). In patients with late onset MTLE-HS, AAO had no contribution to ADC, but seizure

frequency revealed a significantly positive influence on diffusion in the ipsilateral uncinate fasciculus (Table 6, Figure 18B).

Table 6. Multiple linear regression analysis of the ipsilateral WM structures in patients[†].

Groups	Clinical variables	Hemispheric WM	Temporal lobe WM	Uncinate fasciculus
Whole MTLE-HS	AAO	p=0.02 (-0.54)	p=0.001 (-0.70)	p=0.006 (-0.61)
	Age	p=0.009 (+0.58)	ns	p=0.03 (+0.51)
	seizure frequency	ns	ns	ns
	Sex	ns	ns	ns
Early onset MTLE-HS	AAO	p=0.03 (-0.76)	ns	p=0.03 (-0.76)
	Age	ns	ns	ns
	seizure frequency	ns	ns	ns
	Sex	ns	ns	ns
Late onset MTLE-HS	AAO	ns	ns	ns
	Age	ns	ns	ns
	seizure frequency	ns	ns	p=0.03 (+0.75)
	Sex	ns	ns	ns

[†]Results are presented as corrected p values and linear correlation coefficients (r).
MTLE-HS: Mesial-temporal lobe epilepsy with hippocampal sclerosis; WM: white matter; AAO: Age at epilepsy onset; ns: not significant.

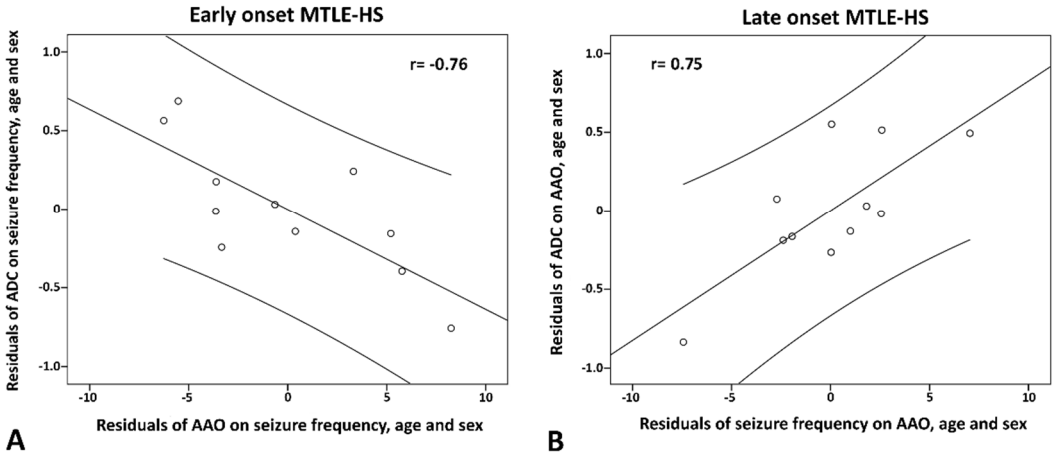

Figure 18. Partial regression plots demonstrating the influence of AAO in early onset disease (A) and seizure frequency in late onset patients (B) on ADC in the ipsilateral uncinate fasciculus. The lines indicate the slope as fitted by linear regression and the 95% confidence intervals. Linear correlation coefficients (r) are also presented.

MTLE-HS: Mesial-temporal lobe epilepsy with hippocampal sclerosis; ADC: Apparent diffusion coefficient; AAO: Age at epilepsy onset.

5.3.A Statistical Model for Intervertebral Disc Degeneration: Determination of the Optimal T2 Cut-Off Values

In total, 21 patients with IVDD were evaluated using midsagittal sections of T2W MR images by three independent neuroradiologists. Among the 105 discs, one disc had to be excluded from further post-processing due to previous low back surgery in the preceding 6 months; therefore, all further analysis could be done on a total of 104 intervertebral discs.

5.3.1. Significance of the Investigated Predictors

The stepwise multiple linear regression analyses revealed that the T2 values and the grades of morphological categories in IVDD were significantly related to age ($p<0.0001$), but no significant association with gender, herniation, and previous low back surgery was found. These independent parameters were not considered as confounding factors in later statistical models.

5.3.2. Intra- and interobserver Reliability

Significant differences were found between the observers in the grading measurements of the Pfirrmann category according to Chi-square analysis (Cramer's V value=0.172; $p=0.018$). In the Schneiderman classification, no differences were found between the observers. During the evaluation of individual grades, the lowest interobserver agreement was found in the Pfirrmann grades III and IV, while the Schneiderman grades 1 and 2 showed moderate and fair agreement (Table 7). Intraobserver agreements in the Pfirrmann scheme were 0.83 (observer A), 0.73 (observer B) and 0.96 (observer C), while the Schneiderman classification showed 0.81, 0.77, and 0.99 kappa values, respectively.

Table 7. Multi-rater generalized kappa values with upper and lower 95% confidence intervals for interobserver agreement.[a]

Classifications	Grades	Kappa	95% Confidence intervals
Pfirrmann	overall	0.46	0.40-0.52
	I	0.77	0.50-1.05
	II	0.40	0.13-0.67
	III	0.33	0.04-0.62
	IV	0.36	0.08-0.64
	V	0.63	0.36-0.90
Schneiderman	overall	0.51	0.45-0.58
	0	0.78	0.50-1.06
	1	0.51	0.24-0.79
	2	0.35	0.04-0.65
	3	0.57	0.28-0.86

[a] Inter-observer reliability is displayed between only the first readings of all observers and calculated among 104 discs.

5.3.3. Quantitative T2 Analysis: Age and Morphological Classifications

The mean T2 value (±SD) in the 104 lumbar discs of IVDD was 78.35±24.20 ms. Multiple linear regression analysis revealed a highly significant inverse correlation between T2 values and age (Figure 19), while the grades of IVDD significantly increased as a function of age (Figure 20 A, B).

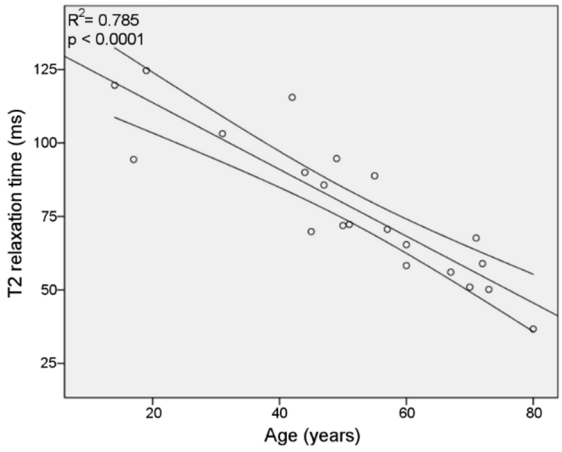

Figure 19 shows the average T2 values as a function of age in patients with IVDD (n=21; the lines indicate the slope as fitted by linear regression and the 95% confidence intervals).

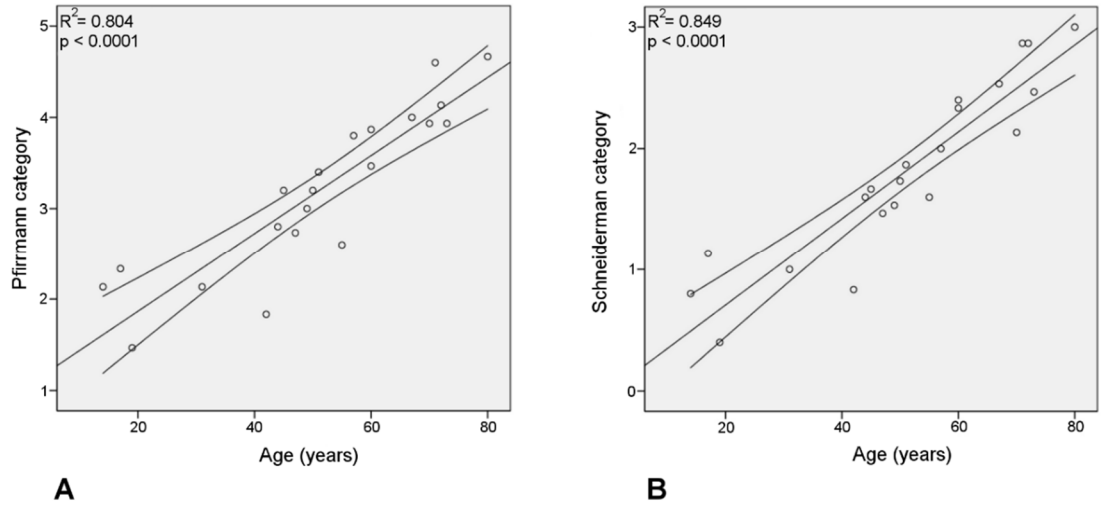

Figure 20. Grading scores as an average of three independent observers revealed a significant elevation of degenerative changes with age according to the Pfirrmann (A) and Schneiderman (B) classifications. The lines indicate the slope as fitted by linear regression and the 95% confidence intervals.

Figure 21 shows the frequency of T2 values in ROIs with different Pfirrmann grades. Grades I/II; II/III, and IV/V were clearly separated from each other, however pronounced overlap was depicted between grades III and IV, which corroborate with low interobserver kappa values.

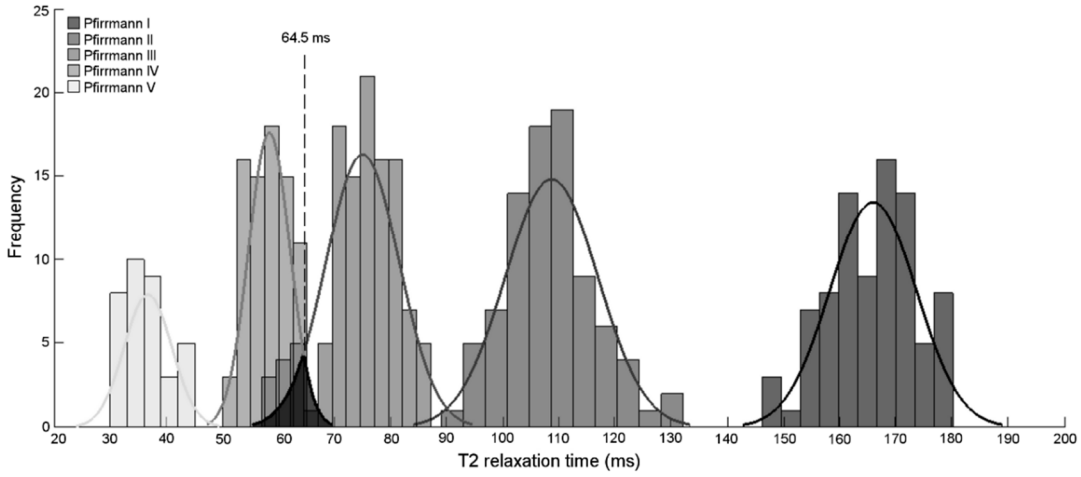

Figure 21 depicts the frequency histogram of T2 values in each Pfirrmann grade. The distribution of T2 values in each Pfirrmann grade shows pronounced overlap between grade III and IV, however the T2 cut-off value (64.5 ms) indicates the degeneration level with 100 % sensitivity and 75 % specificity (Table 8). The number of examined discs, where the decisions of the observers agreed with each other: Pfirrmann I N=9; Pfirrmann II N=6; Pfirrmann III=12; Pfirrmann IV=6; Pfirrmann V=11.

5.3.4. Receiver Operating Characteristic Analysis

Receiver operating characteristic analysis was performed on different Pfirrmann and Schneiderman grades and their cut-off values were calculated. According to the Pfirrmann classification, the T2 ranges of disc degeneration were as follows: grade I (≥119.8 ms), grade II (90.2–119.7 ms), grade III (64.5–90.1 ms), and grade IV (49.0–64.4 ms) grade V (≤48.9 ms). In Pfirrmann grades I/II and II/III T2 cut-off values were determined with 100 % sensitivity and specificity, while these values were somewhat lower, but within the high accuracy range for grades III/IV and IV/V (area under the curve 0.94 and 0.68, respectively). Similar results were observed in the Schneiderman classification scheme, however a significant difference was still apparent between grades 2 and 3 (Table 8).

Table 8. Receiver operating characteristic analysis of T2 cut-off values with regard to morphological classifications.

Categories	Grades	T2 cut-off values (ms)	Sensitivity (%)	Specificity (%)	AUC	p-values
Pfirrmann	I vs II	<119.8	100	100	1	<0.005
	II vs III	<90.2	100	100	1	<0.001
	III vs IV	<64.5	100	75	0.94	<0.05
	IV vs V	<49.0	64	100	0.68	ns
Schneiderman	0 vs 1	<110.3	91	100	0.99	<0.0005
	1 vs 2	<86.3	100	100	1	<0.0001
	2 vs 3	<53.8	65	71	0.74	<0.05

Receiver operating characteristic analysis of the average T2 values was performed among grades when the decisions of the observers agreed with each other. Pfirrmann I N=9, Pfirrmann II N=6, Pfirrmann III N=12, Pfirrmann IV N=6, Pfirrmann V N=11; Schneiderman 0 N=9, Schneiderman 1 N=11, Schneiderman 2 N=14, Schneiderman 3 N=17
AUC: area under the curve

6. Discussion

In the past, the discipline of radiology started with the ability to discern shadows on x-ray images that were abnormal. X-ray imaging was the most modern, state-of-the-art method for a long time but many years later abnormalities can be evaluated on cross-sectional images. Computed tomography and then MR were able to not only observe, but also define and locate the pathological conditions. In the 21st century, neuroimaging has rapidly developed and there was a growing interest for identifying pathologic conditions *in vivo*. Nowadays non-ionizing MRI has a prominent role in imaging and opened a new avenue to study abnormalities in the CNS. MRI is now widespread and generally used qualitatively, however advanced MRI techniques have an increasing role in diagnostics due to the benefits of quantification. The quantification of MR data is possible by using modern image processing tools. The development of such evaluation software packages has been accelerated in the last decade, partly due to the enormous improvement of the scanner hardware but mostly by the revolution in modern information technology.

For the reasons above, a variety of advanced quantitative MRI techniques found their place in clinical practice and in research. These advanced techniques offer more than the anatomical information provided by the conventional MRI sequences. Rather, they generate physiologic data and information on chemical composition. Thus a great variety of disease in the CNS can be judged as macro- and microstructural, metabolic, perfusion or diffusion alterations. By now, advanced MR methods and novel image processing algorithms are considered mature and used to quantitatively evaluate a variety of CNS diseases.

- ***Diffusion alterations in the normal appearing white matter***

DWI is one of the most promising techniques because it is able to detect changes in the brain that are invisible for conventional imaging methods. As stated previously, diffusion can be characterized by a single parameter called ADC, where diffusion related signal decay is assumed to be mono-exponential. However, it has been clearly demonstrated that high b-value diffusion measurements can be fitted to a pair of exponentials (see details in introduction). The analysis of diffusion related signal decay in the NAWM was already performed in different pathological conditions such as MS, tuberous sclerosis, Alzheimer's disease, subarachnoid haemorrhage, leukoaraiosis

(Caramia et al., 2002; Garaci et al., 2004; Hanyu et al., 1997; Liu et al., 2007; Schmidt et al., 2010).

In the past decade our research group has been paying special attention to reveal mono- and bi-exponential diffusion changes in different pathological conditions such as MS, epilepsy, migraine and different brain tumours. It appears that the analysis of diffusion related signal decay and the calculated diffusion parameters provide a sensitive and reliable way to test cellular and subcellular changes that follow pathological conditions. The change in those parameters is usually not specific, but it might unfold morphological/functional characteristics or prior events which are not detected by conventional T1- and T2-weighted imaging. As a consequence, DWI is now routinely included in diagnostic intracranial and extracranial MR protocols in which the mono-exponentially calculated ADC is an important part of the evaluation process.

Recent observations of our research group showed that both mono- and bi-exponential approaches have a role in evaluating NAWM of glioma and meningioma patients. According to this study, the effect of infiltrating tumour cells is not the only reason for the alterations in the NAWM. Complex mechanisms related to the secretory activity of the tumours are also assumed to be important in both infiltrative and non-infiltrative diseases (Horvath et al., 2016b). Although infiltrating tumour cells could be present distant from the tumour itself, the analysis of bi-exponential diffusion data suggested that alterations in the contralateral NAWM of glioma patients might occur mainly as a result of global vasogenic oedema (Horvath et al., 2016a).

It has been also described that diffusion is changing with aging in normal brain (Burgmans et al., 2010; Forbes et al., 2002; Jones et al., 2003; Lee et al., 2009; Mulkern et al., 2001; Naganawa et al., 2003). It was suggested that increased ADC is due to the loss of cellular elements, like neurons, pericytes and axons. In agreement with others (Camara et al., 2007; Forbes et al., 2002; Naganawa et al., 2003; Sala et al., 2012), our bi-exponential study showed an increase of ADC as a function of age in the WM of controls, however fast and slow diffusing components did not change with aging in the interval of 19–51 years. A relative decrease with age was shown in the volume fraction of slow diffusion component. It seems reasonable that the age dependent increase of tissue water diffusion may be caused by a decrease of myelin associated/bound water in control subjects, considering the well-documented age-dependent decrease of myelinated structures (Svennerholm et al., 1997). As for patients with MS, the exact cause of diffusivity changes detected in NAWM is only

partially known. Pathological investigations have identified processes such as glial pathology, axonal loss or perivascular cuffing as the main contributors to NAWM alterations (Miller et al., 2002). In brain specimens, decreased phospholipid levels in myelin structures were demonstrated in NAWM and significant axonal loss was also proved histologically (Moore et al., 2008). The selected MS patients of our study cover a wide range of age with an EDSS score less than 4.0. Although the groups were created according to median age, they did not differ significantly in clinical characteristics listed in Table 1. On the other hand, time interval between last relapse and MRI examination was much longer in the older patient population. This may indicate that the NAWM has undergone recovery during remission resulting in higher lesion number and volume in the younger MS subjects compared with older patients. In spite of the similar functional scores, ADC values were significantly different between younger and older patient groups in most of the NAWM areas.

In MS patients, ADC was inversely related to age, but directly to TLN. This explains the highly significant difference of ADC in the younger age groups, where the mean TLN was generally higher in patients. ADC was significantly different in all participants group of patients compared with controls, maybe due to the altered diffusion in younger patients. In older patient group, ADC was not significantly different compared to controls.

Our findings are in agreement with others (Caramia et al., 2002), where significant correlation was revealed between TLN and ADC in NAWM of MS patients. Accordingly, it has been suggested that the primary reason for ADC increase in NAWM of MS patients is the activity of the disease that manifests with elevation of hyperintense lesions (Meier et al., 2007) and abnormal myelination. The results of bi-exponential analysis showed that ADC_f and ADC_s are independent as a function of TLN and age. Contrary to ADC, f_s is directly proportional to age, but inversely related to TLN in MS patients. It seems reasonable that the frequency of WM lesions might reflect diffusion alterations in the NAWM. We found that f_s values of MS patients decreased by about 7-11% compared to healthy controls. It may be an indirect effect of myelin water fraction change, but the attribution of f_s solely to myelin water fraction is highly speculative (MacKay et al., 1994). Of course, even more alternatives can also be considered responsible for the observed change in diffusion MRI metrics.

Besides multiple sclerosis, NAWM changes are also relevant but less known in temporal lobe epilepsy. However, some studies focus on specific individual WM tracts

and make inferences about microstructural integrity of axons and myelin sheaths through the analysis of diffusivity perpendicular and parallel to the tracts. In our previous study, we found that the AAO may distinguish different clinical subgroups in MTLE-HS (Janszky et al., 2004). The AAO is commonly associated with clinical and semiological dissimilarities (Janszky et al., 2004; Villanueva and Serratosa, 2005). Although the age at first non-provoked seizure can have a decisive effect on brain tissues in MTLE-HS, limited data exist regarding WM diffusion changes with respect to the epilepsy-related clinical parameters such as AAO and chronic seizure activity.

Previous studies examined the presence and the extent of WM abnormalities in temporal lobe epilepsy. According to them, WM differences in patients were detectable compared with healthy controls, but they were more pronounced in the group with early onset MTLE-HS (Riley et al., 2010; Villanueva and Serratosa, 2005). Additionally, the earlier AAO rather than the duration of the disease was associated with reduced cerebral WM volume and it was not related to initial precipitating injury, occurrence/number of generalized seizures, and number of antiepileptic drugs (Hermann et al., 2002). Beyond the volumetric studies, there have been numerous reports based on diffusion imaging in adult patients with temporal lobe epilepsy in which bilateral WM alterations can usually be detected in the limbic and nonlimbic areas with ipsilateral predominance (Concha et al., 2009; Concha et al., 2005; Focke et al., 2008; Gross et al., 2006; Kim et al., 2008; Lin et al., 2008; Riley et al., 2010). These changes are more extensive in patients with mesiotemporal sclerosis than in the nonlesional group (Concha et al., 2009; Scanlon et al., 2013). Although the underlying cause is not clear for such alterations, several possible theories exist. According to one hypothesis, these changes may be the result of neuronal loss in epileptic foci causing secondary axonal degeneration far away from the seizure focus. There are important frontotemporal tracts or other pathways connecting the two temporal lobes or hemispheres (e.g., uncinate fasciculi, arcuate fasciculi, corpus callosum) which are commonly associated with diffusion alterations. These are frequently involved in seizure propagation from the temporal lobe and might explain the role of recurring epileptic activity with abnormal neuronal firing on WM abnormalities. Findings of WM diffusion alterations have also been complemented by GM disruption. The extent of GM disruption is closely related to the start of the disease (Kemmotsu et al., 2011) and also more severe in regions that are anatomically and functionally connected to the hippocampus (Bernasconi et al., 2005; McDonald et al., 2008). An extensive

literature has shown disruptions in interregional fibre diffusivity in the mesiotemporal and the frontotemporal networks (Ahmadi et al., 2009; Rodrigo et al., 2007) and in the speech-dominant hemisphere (Powell et al., 2007) suggesting decreased fibre arrangement and altered myelin membranes. These findings support the hypothesis that GM volume loss and WM damage may be related to each other and probably due to the excitotoxic effects of spreading epileptogenic activity in brain regions that are directly or indirectly connected to the hippocampus. Our results revealed that ADC derived from the ipsilateral hemispheric WM of patients with MTLE-HS was higher compared with that from the corresponding side of controls. These are consistent with previous findings suggesting that WM abnormalities are most pronounced in the cerebral hemisphere ipsilateral to the seizure focus (Ahmadi et al., 2009; Otte et al., 2012; Riley et al., 2010). Additionally, ADC of patients with early onset MTLE-HS was elevated not only in the ipsilateral hemispheric but also in the ipsilateral temporal lobe WM compared with that of controls; however, these differences were not detectable in the group with late onset MTLE-HS. According to animal and human studies, the impairment of WM is related to age at recurrent seizure onset and being more severe when seizures appeared at younger ages (Hermann et al., 2002; Sayin et al., 2015). This could be explained either by a primary pathology or by different neurodevelopmental processes precipitating epilepsy. However, it cannot be ruled out that the adverse effect of the recurrent seizures in the developing, immature brain might lead to WM impairment in early onset epilepsy. Indeed, myelination and the consequent cerebral volume increase is a long-lasting event and occurs in the hippocampus and in the cerebral WM beyond the age of 16 (the age limit of the group with early onset MTLE-HS in our study) (Suzuki et al., 2005). In addition, we found that ADC of the group with early onset MTLE-HS was negatively related to AAO in the ipsilateral hemispheric WM and the uncinate fasciculus. But in the group with late onset MTLE-HS, the seizure frequency had a positive influence on ADC in the ipsilateral uncinate fasciculus. It could be assumed that different pathophysiological mechanisms (such as seizure-related injury as well as epileptogenesis) and etiological factors do not equally participate in WM degeneration.

- ***The quantification of intervertebral disc degeneration***

Since IVDD is thought to be a major factor that results in lumbar pain, follow-up of the degenerative process is a common morphological aspect that should be

considered. Altered morphology can be measured as a change of size/shape or the change of pixel intensities on the radiographic image (de Schepper et al., 2010; Pye et al., 2007; Pye et al., 2004). Consequently, several grading systems have been worked out in the past including those which utilize MR images, primarily from T2W measurements. MR imaging classifications such as the Schneiderman (Schneiderman et al., 1987) and the modified Pfirrmann scheme designed for both elderly (Griffith et al., 2007) and young subjects (Takatalo et al., 2011) while other classifications have been developed for more specific changes (Aprill and Bogduk, 1992; Fardon et al., 2001; Modic et al., 1988; Yu et al., 1988). Today, the most accepted grading system of IVDD is that of Pfirrmann et al. which is a semiquantitative grading based on the T2W signal changes of the NP and the height of lumbar discs, sorting them in five categories (Pfirrmann et al., 2001). Despite these justified morphological standards, the measurements of IVDD on T2W images may hide important features (Takashima et al., 2012; Watanabe et al., 2007). Consequently, the visual perception of signal intensity on T2W images is problematic which may lead to differences between the observers, especially when they have different levels of experience and areas of expertise or the examiners show overall variation in stringency. These prior sources of disagreement will be reflected in dissimilarity between the observers (Sim and Wright, 2005), as a consequence, interobserver differences appear. Nevertheless, the interobserver agreement is frequently calculated between two observers at once even though more raters are involved in the study (Lurie et al., 2008; Pfirrmann et al., 2001). In fact, most of the studies in current literature measure intra- and interobserver reliabilities based on the Pfirrmann classification system, however they show a high variation depending on the backgrounds, the number of observers and last but not least the consensus based decision (Table 9) (Arana et al., 2010; Carrino et al., 2009; Griffith et al., 2007; Hangai et al., 2009; Kettler and Wilke, 2006; Lurie et al., 2008; Pfirrmann et al., 2001; Watanabe et al., 2007; Yu et al., 2012). Therefore the comparison is difficult and easily leads to confusion.

Table 9. Intra- and interobserver agreement of lumbar disc degeneration with regard to the Pfirrmann grading system

Corresponding paper	Publication date	Observers	Intraobserver agreement	Interobserver agreement
Pfirrmann et al.	2001	1 orthopedic surgeon 2 musculoskeletal radiologists	0.84-0.90	0.69-0.81
Griffith et al.	2007	2 musculoskeletal radiologists 1 general radiologist	0.79-0.91	0.65-0.67
Watanabe et al.	2007	3 experienced observers	0.74-0.90	0.70-0.74
Carrino et al.	2009	3 musculoskeletal radiologists 1 orthopedic spine surgeon	0.57-0.88	0.56-0.76
Lurie et al.	2008	3 musculoskeletal radiologists 1 orthopedic spine surgeon	0.44-0.83	mean of 0.47
Yu et al.	2012	2 orthopedic surgeons	0.82-0.89	0.70-0.82
Arana et al.	2010	5 radiologists	mean of 0.69	mean of 0.49
Hangai et al.	2008	2 orthopedic surgeons	mean of 0.90	mean of 0.87

Both intra- and interobserver agreements are displayed with kappa values.

The discrimination of grades on morphological images is not always possible with full agreement. The morphological T2W image of the lumbar spine shows only the cross-sectional information of the T2 relaxation curve. On the contrary, T2 relaxometry quantitatively describes the whole T2 relaxation process and provides one of the most reliable correlations with the changes of molecular environment in the disc (Niu et al., 2011). Despite these facts, only one study has suggested that T2 relaxation time evaluation may have a role to determine the range of T2 values for disc degeneration (Takashima et al., 2012).

In our study, the possibility of quantitative classification in IVDD was investigated: T2 cut-off values, intra- and interobserver reliability with regard to morphological classifications of the Pfirrmann and Schneiderman schemes were determined. Similarly to others, (Marinelli et al., 2010; Niu et al., 2011; Stelzeneder et al., 2012) our results showed that the T2 relaxation time of lumbar intervertebral discs decreased with increasing morphological grades and age, likely reflecting a decrease in proteoglycan and water content (Haneder et al., 2013; Urban and McMullin, 1988; Zou et al., 2009). Only moderate overall agreement was found between the observers in both the Pfirrmann and Schneiderman classification systems regarding the interobserver reliability, while intraobserver agreement was substantial to almost perfect. Between Pfirrmann grades III and IV a pronounced overlap was observed in T2 values, which corroborates with a low interobserver kappa coefficient. The use of receiver operating characteristic analysis among grades of IVDD yields quantitative T2 cut-off values. They can be determined with an approximate reliability from the

area under the curve (Takashima et al., 2012), which were within substantial to almost perfect accuracy level (0.68–1) in this study. These data indicate that this quantitative grading is a more powerful way to evaluate IVDD, even if the interobserver reliability is low.

6.1. Limitations

- ***Bi-exponential diffusion signal decay in normal appearing white matter of multiple sclerosis***

We should emphasize that one major limitation of the study was the limited number of patients and controls involved; therefore small sample sizes were examined in subgroups dichotomized by the median age. A wider age range would have been also beneficial, – the EDSS, as an inclusion criterion was kept relatively low – but older patients with MS mostly suffer from more disability, which may result higher EDSS leading to a big difference in the measured data (Alajbegovic et al., 2009).

To date, several DWI study analyses were done at least partially based on region of interest method which requires a prior assumption of the region to be evaluated. On the other hand, voxel-based methods are also available which could allow whole brain analyses of our diffusion data (Cohen et al., 2009; Scherfler et al., 2006; Smith et al., 2006). However, these methods are dependent on perfect nonlinear registration and the extent of applied smoothing or require diffusion tensor imaging data for the calculation (Smith et al., 2006).

Using trace-weighted images (via geometric averaging of the measurements along the three orthogonal directions) for bi-exponential analysis can lead to cross terms, which may entangle the bi-exponential parameters (Maier et al., 2010; Maier et al., 2004; Mulkern et al., 2001). Because these cross-terms may vary if another set of orthogonal directions are used, rotational invariance is brought into question in the context of bi-exponential fitting.

Despite these limitations, our results measured in NAWM show a very good overall agreement with the literature both in control subjects and MS patients.

- ***Age at onset and seizure frequency affect white matter diffusion coefficient in patients with mesial temporal lobe epilepsy***

The current study has some limitations. (1) One of the limitations is the low number of patients and controls involved. Apparent diffusion coefficient in the ipsilateral temporal lobe of patients with early onset MTLE-HS tended to decrease as a function of AAO, but no significant correlation was found between them. Probably, the effect of AAO averaged out leaving no difference in diffusion because of the relatively small number of observations and large number of predictors. (2) In this study, only 13 of the 22 patients underwent an adult presurgical evaluation protocol, therefore the possibility of subtle bilateral disease cannot be ruled out. (3) In order to perform powerful statistical analysis, patients were divided into two groups according to the median AAO (i.e. groups with early and late onset MTLE-HS). Although no significant differences were observed in clinical and demographic data (e.g., seizure frequency, level of education), the comparison of WM diffusivity between the groups with early and late onset MTLE-HS may be problematic because of the atypical average AAO of patients with late onset MTLE-HS. (4) The frequency of seizures may change over years in patients with MTLE-HS, which can also have dominant influence on WM integrity. To shed light on this relationship, a longitudinal study is needed using a larger patient population. (5) Since subtle abnormalities may remain hidden with hemispheric and lobar approaches, particularly when they occur in small fractions of the brain, we performed diffusion analysis also in the tracts connected to the temporal lobe. In spite of this, diffusion tensor imaging would have been beneficial to investigate tract based WM deviation.

- ***A Statistical Model for Intervertebral Disc Degeneration: Determination of the Optimal T2 Cut-Off Values***

The current study might have some limitations. First, the selection of ROIs may be a source of bias, especially when ROIs were drawn for the T2 measurements by a single observer whose results were compared with morphological classifications carried out by several investigators. Also, the magnitude of error caused by the manually delineated ROIs might lead to inaccurate T2 values in the discs. This could have introduced subjectivity and bias, mainly when the central region is poorly differentiated from the annulus fibrosus in discs with higher degeneration grades. It is

possible to avoid manual segmentation of the lumbar discs by using intensity based automatic and semi-automatic methods like watershed transform and live wire segmentation (Claudia et al., 2012), but still manual interaction remains a necessity in many cases. Second, for most quantitative MRI based T2 studies like this, there has been a tendency to assume mono-exponential T2 decay to derive T2 relaxation times from tissues. However, CPMG imaging sequences with optimized non-selective (hard) or selective (soft) refocusing pulses and larger time frames (up to TE of 320 ms) have also proven capable to extract more accurate multi-exponential T2 decay curves (Mulkern et al., 1990), which might hold additional information regarding the underlying biology of the discs.

7. Conclusions

According to our first study, the decreased volume fraction of slow diffusing component may be the primary reason for the age-dependent increase of ADC in controls. In multiple sclerosis, the diffusion parameters are related to both age and total lesion number, in which the bi-exponential analysis indicated decreased f_s as a function of total lesion number while it increased with age, probably due to the reduction of myelin water fraction. These data demonstrated that the myelin content of the WM affects diffusion in relapsing-remitting MS that is possibly a consequence of the shift between different water fractions.

In mesial-temporal lobe epilepsy, the timing of disease seems to be the major origin of WM abnormalities in early onset epilepsy, while in late onset disease it should be assumed as a secondary effect provoking diffusion changes. The combination of clinical data and novel MR methods used in our study has led to valuable insights into epilepsy-associated changes in the WM and has increased our understanding of the pathophysiology of mesial-temporal lobe epilepsy.

Our T2 relaxometry study reflected that T2 values tended to decrease with increasing age or grade in the NP possibly due to the decrease of water and proteoglycan content. Interobserver agreement of the morphological evaluation in patients with IVDD was only fair between Pfirrmann III and IV. Based on our results, quantitative T2 cut-off values seem to be a more reliable method to define the degree of disc degeneration, even though the definitions of intervertebral disc degeneration in MRI are still not uniform.

8. Current trends and brief summary

Many imaging modalities and techniques exist to assess alterations in the CNS. MRI is one of the most popular ones because it does not employ ionizing radiation. On the other hand, subtle changes can be invisible for human perception even on clinical MR images, but advanced quantitative MRI methods are capable to delineate molecular alterations. Conventionally invisible condition is the so called normal appearing grey/white matter and usually unaccounted for in clinical radiology. Previous studies stated that the examination of NAWM has an important role in diagnosing, prognosing and grading of a specific disease. Grading/staging is often linked to therapeutic protocols in which quantitative imaging plays an increasing role. DWI is a quantitative method of choice to clarify the nature of diffusion alterations in the NAWM of glioma. According to the recent results of our research group, both infiltrative and non-infiltrative tumours have shown altered diffusion in the NAWM, which is not exclusively caused by tumour infiltration but also related to global vasogenic oedema and the secretory activity of the tumours (Horvath et al., 2016a; Horvath et al., 2016b). Advanced neuroimaging techniques have found to be promising in other neurological conditions such as infections, brain lymphomas, traumatic brain injuries, MS and epilepsy. Out of these, MS and temporal lobe epilepsy were examined in the current thesis using DWI, but other advanced methods also exist. In multiple sclerosis, novel quantitative MR techniques were recently developed to quantify the extent and characterize the nature of structural changes occurring within and outside focal lesions. Advanced diffusion tensor imaging has spurred the development of brain neuroconnectivity techniques, which define and quantify anatomic links between remote brain regions by axonal fibre pathways (Li et al., 2013). Other imaging techniques like perfusion and functional MRI allow the assessment of hemodynamic abnormalities and improve the understanding of cortical reorganization after tissue injury (Filippi et al., 2013; Francis et al., 2013). However, functional abnormalities have also been examined using positron emission tomography (Kiferle et al., 2011), while a novel approach called diffusion tensor spectroscopy investigate diffusion properties of intracellular, cell type specific metabolites in the NAWM at 7 T scanner (Wood et al., 2012). As for epilepsy patients, fMRI has gained widespread acceptance to establish hemispheric language dominance and evaluating the potential damage caused to eloquent areas related to the epileptogenic focus, while morphometric MRI

analysis based on novel image processing algorithms is able to highlight brain areas with blurred grey-white matter junction and abnormal gyration (Wagner et al., 2011). Additionally, simultaneous EEG and functional MRI can allow the mapping of haemodynamic networks over the entire brain related to specific spontaneous and triggered epileptic events and thereby provide new localizing information (van Graan et al., 2015). Also the semi-quantitative analysis of positron emission tomography data and the co-registered MR image help to identify mild abnormalities.

Advanced imaging methods are also used outside the brain and they are increasingly supplementing the traditional approaches. Quantitative MR measurements of the intervertebral discs – such as T1rho, T2 relaxometry and dGEMRIC – have been correlated with biochemical content, biomechanical function and even discogenic pain (Hwang et al., 2016), while ultrashort echo time imaging offer additional way for the evaluation of health and injury of the lumbar spine (Hwang et al., 2016). The above list of advanced imaging techniques is not exhaustive, so other methods and image processing algorithms exist in the brain and even beyond that (Sacerdoti et al., 2016), (https://www.ncbi.nlm.nih.gov/pmc/journals/1905/).

Altogether, this thesis gives an inside view of advanced MRI techniques and their image processing methods in the CNS. Today, neuroimaging goes on its own way and it has already changed our society, but how far can it go? Will we ever understand how the human brain works?

9. Acknowledgements

All the work presented in this thesis could not have been carried out without the enormous help from numerous people, to whom I owe a great debt of gratitude.

First, I would like to thank my supervisor Prof. Péter Bogner for the continuous support, guidance and advices he has provided throughout my time as his radiographer student. I have been extremely lucky to have a supervisor who cared so much about my work as the best mentor from the very beginning. I would also like to emphasize my deep gratitude towards Prof. Tamás Dóczi and Dr. Ferenc Kövér for the financial and technical support of my work. I am beholden to Prof. József Janszky, Prof. Boldizsár Czéh and Dr. Hajnalka Ábrahám for their continuous help and great advices. I must thank to Dr. Mihály Aradi who also guided me when I was a bachelor student and answered dozens of questions tirelessly. I want to express my deep appreciation for the help, kindness and critical point of view to my colleagues Dr. Gábor Perlaki

and Dr. Gergely Orsi. Without their help, I doubt I would have been able to complete the project in such a manner. I would also like to thank all the members of staff at Diagnostic Centre of Pécs and University of Pécs, especially to Dr. Réka Horváth, Dr. Andrea Horváth, Kristóf Biczó and Péter Bódi for their continuous help and support. I owe special thanks to the radiographers, radiologists, receptionists, administrators and assist members of Diagnostic Centre of Pécs for their help and kindness. I am also grateful to my PhD colleagues in particular Dr. Enikő Plózer, Dr. Anna Altbäcker, Dr. Gergely Darnai and Dr. Arnold Tóth to their help and friendship.

Last but not least, I am grateful for the love encouragement and tolerance of Attila Hajnal, the man who staying by my side through all the ups and downs. Without his patience and sacrifice, I could not have completed this thesis. A special word of thanks also goes to my family for their continuous support and encouragement.

10. Publications

Articles related to the thesis

Nagy S.A.[*], Horvath R.[*], Perlaki G., Orsi G., Barsi P., John F., Horvath A., Kovacs N., Bogner P., Abraham H., Bone B., Gyimesi C., Doczi T., Janszky J. Age at onset and seizure frequency affect white matter diffusion coefficient in patients with mesial temporal lobe epilepsy (2016). Epilepsy Behav 61:14-20. **IF: 2.332**
[*]Equal contribution in first authorship

Nagy S.A.[*], Juhasz I.[*], Komaromy H., Pozsar K., Zsigmond I., Perlaki G., Orsi G., Schwarcz A., Walter N., Doczi T., Bogner P. A statistical model for intervertebral disc degeneration: determination of the optimal T2 cut-off values (2014). Clin Neuroradiol 24:355-63. **IF: 2.250**
[*]Equal contribution in first authorship

Nagy S.A., Aradi M., Orsi G., Perlaki G., Kamson D.O., Mike A., Komaromy H., Schwarcz A., Kovacs A., Janszky J., Pfund Z., Illes Z., Bogner P. Bi-exponential diffusion signal decay in normal appearing white matter of multiple sclerosis (2013). Magn Reson Imaging 31:286-95. **IF: 2.022**

Articles unrelated to the thesis

Khan M.I.H., Wellard R.M., **Nagy S.A.**, Joardder M.U.H., Karim M.A. Experimental investigation of bound and free water transport process during drying of hygroscopic food material (2017). Int J Therm Sci. 117:266-273. **IF: 2.769**

Altbacker A., Plozer E., Darnai G., Perlaki G., Horvath R., Orsi G., **Nagy S.A.**, Bogner P., Schwarcz A., Kovacs N., Komoly S., Clemens Z., Janszky J. Problematic internet use is associated with structural alterations in the brain reward system in females (2016). Brain Imaging Behav 10:953-959. **IF: 3.667**

Darnai G., Plózer E., Altbácker A., Perlaki G., Orsi G., Kőszegi T., **Nagy S.A.**, Lucza T., Kovács N., Janszky J., Zsófia C. The relationship between serum cholesterol and verbal memory may be influenced by body mass index (BMI) in young healthy women (2016). Ideggyogy Sz. 69:177-82. **IF: 0.376**

Darnai G., Plozer E., Perlaki G., Orsi G., **Nagy S.A.**, Horvath R., Schwarcz A., Kovacs N., Altbacker A., Janszky J., Clemens Z. 2D:4D finger ratio positively correlates with total cerebral cortex in males (2016). Neurosci Lett 615:33-6. **IF: 2.107**

Horvath A., Perlaki G., Toth A., Orsi G., **Nagy S.A.**, Doczi T., Horvath Z., Bogner P. Increased diffusion in the normal appearing white matter of brain tumor patients: is this just tumor infiltration? (2016). J Neurooncol 127:83-90. **IF: 2.754**

Horvath A., Perlaki G., Toth A., Orsi G., **Nagy S.A.**, Doczi T., Horvath Z., Bogner P. Biexponential diffusion alterations in the normal-appearing white matter of glioma patients might indicate the presence of global vasogenic edema (2016). J Magn Reson Imaging 44:633-41. **IF: 3.250**

Khan M.I.H., Wellard R.M., **Nagy S.A.**, Joardder M.U.H., Karim M.A. Investigation of bound and free water in plant-based food material using NMR T2 relaxometry (2016). Innovative Food Science & Emerging Technologies 38:252-261. **IF: 2.997**

Perlaki G., Szekeres S., Orsi G., Papp L., Suha B., **Nagy S.A.**, Doczi T., Janszky J., Zambo K., Kovacs N. Validation of an automated morphological MRI-based (123)I-FP-CIT SPECT evaluation method (2016). Parkinsonism Relat Disord 29:24-9. **IF: 3.794**

Aschermann Z., Perlaki G., Orsi G., **Nagy S.A.**, Horvath A., Bone B., Bihari K., Acs P., Janszky J., Komoly S., Bogner P. Quantitative assessment of brain iron by R2* relaxometry in patients with cervical dystonia (2015). Mov Disord 30:1422-6. **IF: 6.010**

Bardos T., Vancsodi J., Farkas B., Fazekas A., **Nagy S.A.**, Bogner P., Vermes C., Than P. Pilot Study of Cartilage Repair in the Knee Joint with Multiply Incised Chondral Allograft (2015). Cartilage 6:73-81. **IF: 1.127**

Darnai G., Plozer E., Perlaki G., Orsi G., **Nagy S.A.**, Horvath R., Schwarcz A., Kovacs N., Altbacker A., Janszky J., Clemens Z. Milk and dairy consumption correlates with cerebral cortical as well as cerebral white matter volume in healthy young adults (2015). Int J Food Sci Nutr 66:826-9. **IF: 1.451**

Erdelyi-Botor S., Aradi M., Kamson D.O., Kovacs N., Perlaki G., Orsi G., **Nagy S.A.**, Schwarcz A., Doczi T., Komoly S., Deli G., Trauninger A., Pfund Z. Changes of migraine-related white matter hyperintensities after 3 years: a longitudinal MRI study (2015). Headache 55:55-70. **IF: 2.961**

Horvath A.*, **Nagy S.A.***, Perlaki G., Orsi G., Bogner P., Doczi T. Multimodal Quantitative Characterization of Intracranial Epidermoid Cysts: Preliminary Results (2015). Ideggyogy Sz 68:347-55. **IF: 0.376**
*Equal contribution in first authorship

Orsi G., Aradi M., **Nagy S.A.**, Perlaki G., Trauninger A., Bogner P., Janszky J., Illes Z., Doczi T., Pfund Z., Schwarcz A. Differentiating white matter lesions in multiple sclerosis and migraine using monoexponential and biexponential diffusion measurements (2015). J Magn Reson Imaging 41:676-83. **IF: 3.250**

Plozer E., Altbacker A., Darnai G., Perlaki G., Orsi G., **Nagy S.A.**, Schwarcz A., Koszegi T., Woth G.L., Lucza T., Kovacs N., Komoly S., Clemens Z., Janszky J. Intracranial volume inversely correlates with serum 25(OH)D level in healthy young women (2015). Nutr Neurosci 18:37-40. **IF: 2.616**

Perlaki G., Orsi G., Plozer E., Altbacker A., Darnai G., **Nagy S.A.**, Horvath R., Toth A., Doczi T., Kovacs N., Bogner P., Schwarcz A., Janszky J. Are there any gender differences in the hippocampus volume after head-size correction? A volumetric and voxel-based morphometric study (2014). Neurosci Lett 570:119-23. **IF: 2.030**

Vaczi M., **Nagy S.A.**, Koszegi T., Ambrus M., Bogner P., Perlaki G., Orsi G., Toth K., Hortobagyi T. Mechanical, hormonal, and hypertrophic adaptations to 10 weeks of eccentric and stretch-shortening cycle exercise training in old males (2014). Exp Gerontol 58:69-77. **IF: 3.485**

Aradi M., Schwarcz A., Perlaki G., Orsi G., Kovacs N., Trauninger A., Kamson D.O., Erdelyi-Botor S., Nagy F., **Nagy S.A.**, Doczi T., Komoly S., Pfund Z. Quantitative MRI studies of chronic brain white matter hyperintensities in migraine patients (2013). Headache 53:752-63. **IF: 3.189**

Yadamsuren E.A., **Nagy S.A.**, Pajor L., Lacza A., Bogner B. Characteristics of advanced- and non advanced sporadic polypoid colorectal adenomas: correlation to KRAS mutations (2012). Pathol Oncol Res 18:1077-84. **IF: 1.555**

Nagy S.A., Aradi M., Pfund Z., Orsi G., Perlaki G., Bogner P. Regionális látszólagos diffúziós koefficiens változások az életkor függvényében normál és sclerosis multiplex csoportokban. EGÉSZSÉG-AKADÉMIA (2010). 1:239-247. **IF: -**

Oral and poster presentations related to the thesis

Nagy S.A., Fehérállományi diffúziós eltérések temporális lebeny epilepsziában – az életkori kezdet hatásai. II. Idegtudományi Centrum/Szentágothai János Kutatóközpont PhD és TDK konferencia (2015.11.5-6.). Pécs, Hungary (Conference winner and best presentation award)

Nagy S.A., Horvath R., John F., Janszky J., Perlaki G., Doczi T., Bogner P. Age at onset effect on white matter diffusion coefficient of temporal lobe epilepsy patients. ESMRMB Congress (2015.10.01-03.). Edinburgh, UK, (Poster and oral presentation)

Nagy S.A., John F., Horvath R., Janszky J., Perlaki G., Orsi G., Barsi P., Bogner P. Age at onset effect on white matter diffusion coefficient of temporal lobe epilepsy patients. Neuroimaging workshop (2015.04.17-18.). Szeged, Hungary

Nagy S.A., Horvath R., John F., Janszky J., Perlaki G., Horvath A., Bogner P. Legújabb MR módszerek és alkalmazási területeik különböző intracraniális betegségekben. X. IME Jubileumi Képalkotó Diagnosztikai Továbbképzés és Konferencia (2015.03.26.). Budapest, Hungary

Nagy S.A., John F., Horvath R., Perlaki G., Orsi G., Barsi P., Dóczi T., Kover F., Janszky J., Bogner P. Bi-exponential diffusion signal changes in mesial temporal lobe epilepsy and juvenile myoclonic epilepsy. A Magyar Neuroradiológiai Társaság XXII. Kongresszusa (2014.11.06-08.). Hajduszoboszló, Hungary

Nagy S.A. „Láthatatlan" eltérések vizsgálata, avagy post processing epilepsziában. A Magyar Radiológus Asszisztensek Egyesületének XVIII. Kongresszusa (2014.09.25-27.). Kaposvár, Hungary

Nagy S.A., Horvath R., Perlaki G., Plozer E., Orsi G., Janszky J., Doczi T., Kasprian G., Woitek R., Bogner P. Bi-exponential diffusion signal alterations in mesial temporal lobe epilepsy. A Magyar Neuroradiológiai Társaság XXI. Kongresszusa (2013.11.07-09.). Visegrád, Hungary

Nagy S.A., Horvath R., Perlaki G., Plozer E., Orsi G., Janszky J., Doczi T., Bogner P. Bi-exponential diffusion signal alterations in mesial temporal lobe epilepsy – initial results. ISMRM Scientific Workshop (2013.10.14-18.) Podstrana, Croatia (Poster presentation)

Nagy S.A., Juhasz I., Komaromy H., Pozsar K., Zsigmond I., Perlaki G., Orsi G., Schwarcz A., Janszky J., Bogner P. A statistical model for intervertebral disc degeneration: determination of the optimal T2 cut-off values. Neuroimaging Workshop (2013.04.19-20.). Pécs, Hungary

Nagy S.A., Juhasz I., Komaromy H., Pozsar K., Zsigmond I., Perlaki G., Orsi G., Aradi M., Perlaki G., Orsi G., Bogner P. Classification of intervertebral disk degeneration using quantitative T2 relaxation time measurements. European Congress of Radiology (2013.03.07-11.).Vienna, Austria (Electronic poster)

Nagy S.A., Bogner P., Aradi M., Orsi G., Perlaki G., Komaromy H., Schwarcz A., Janszky J. Bi-exponential diffusion signal decay in normal appearing white matter of multiple sclerosis. 16th EFNS Congress (2012.09.08-11.). Stockholm, Sweden (Poster presentation with oral discussion)

Komaromy H., Juhasz I., **Nagy S.A.**, Pozsar K., Zsigmond I., Aradi M. The comparison of morphological and quantitative MR classification of intervertebral disc degeneration using the evaluation of independent neuroradiologist readers. A Magyar Neuroradiológiai Társaság XX. Kongresszusa (2012.11.08-10.). Eger, Hungary

Nagy S.A., Mike A., Komaromy H., Aradi M., Perlaki G., Orsi G., Bogner P. Quantitative MRI in acut multiple sclerosis relapse. A Magyar Neuroradiológiai Társaság XX. Kongresszusa (2012.11.08-10.). Eger, Hungary

Juhasz I., Aradi M., **Nagy S.A.**, Papp M., Perlaki G., Orsi G., Toth A., Nagy Gy., Bogner P. Classification of intervertebral disk degeneration using quantitative T2 relaxation time measurements. A Magyar Neuroradiológiai Társaság XX. Kongresszusa (2012.11.08-10.). Eger, Hungary

Nagy S.A., Bogner P., Juhasz I., Komaromy H., Pozsar K., Zsigmond I., Aradi M., Perlaki G., Orsi G. Degeneratív porckorongbetegség kvantitatív MR vizsgálata: Klasszifikáció másképpen. A Magyar Radiológus Asszisztensek Egyesületének XVII. Kongresszusa (2012.10.11-13.). Miskolc, Hungary

Aradi M., **Nagy S.A.**, Juhasz I., Papp M., Perlaki G., Orsi G., Toth A., Nagy Gy., Schwarcz A., Bogner P. Degeneratív porckorongbetegség vizsgálata kvantitatív T2 MR mérésekkel. A Magyar Radiológusok Társasága XXVI. Kongresszusa (2012. 06. 21-23.). Debrecen, Hungary

Nagy S.A., Bogner P., Aradi M., Orsi G., Perlaki G., Schwarcz A. Bi-exponenciális diffúzió a normál megjelenésű fehérállományban: az öregedés és léziótömeg hatása sclerosis multiplexben. A Magyar Neuroradiológiai Társaság XIX. Kongresszusa (2011.10.27-29.). Velence, Hungary

Nagy S.A., Az agyszöveti vízdiffúzió életkori változása egészséges és sclerosis multiplexes csoportokban. A XXX. Országos Tudományos Diákköri Konferencia Orvos- és Egészségtudományi Szekciója (2011.04.07-09.). Debrecen, Hungary (Third place and special award)

Nagy S.A. Az agyszöveti vízdiffúzió életkori változása egészséges és sclerosis multiplexes csoportokban. Baranya megyei Szakdolgozók V. Tudományos Napja (2010.11.30.). Pécs, Hungary

Nagy S.A., Aradi M., Orsi G., Perlaki G., Pfund Z., Bogner P. Kvantitatív diffúziós MR képalkotás alkalmazása az agyszöveti vízdiffúzió életkori változásának követésében. A Magyar Radiológus Asszisztensek Egyesületének XV. Kongresszusa (2010.09.24-25.). Budapest, Hungary

Nagy S.A. Az agyszöveti vízdiffúzió életkori változása egészséges és sclerosis multiplexes csoportokban. XVI. Kari Tudományos Diákköri Konferencia (2010.04.23-24.). Szombathely, Hungary (First place and special award)

Oral and poster presentations unrelated to the thesis

Nemeth N., **Nagy S.A.**, Czeh B., Doczi T., Bogner P., Miseta A., Tenyi T., Simon M. Agyi funkcionális MR eltérések kori traumán átesett depressziós betegekben. A Magyar Pszichiátriai Társaság XXI. Vándorgyűlése (2017.01.26-28.). Siófok, Hungary (Poster presentation)

Nemeth N., **Nagy S.A.**, Bogner P., Doczi T., Miseta A., Czeh B., Simon M. A face-emotion fMRI paradigm to activate the amygdala in early traumatized adults with depression. IBRO Workshop, Hungarian Academy of Science (2016.01.21-22.). Budapest, Hungary (Poster presentation)

Nagy S.A., Nemeth N., Bogner P., Miseta A., Doczi T., Czeh B., Simon M. Resting-state functional connectivity alterations in depressed subjects with childhood trauma. A pilot study. IBRO Workshop, Hungarian Academy of Science (2016.01.21-22.). Budapest, Hungary (Poster presentation)

Orsi G., Perlaki G., Horvath R., **Nagy S.A.**, Toth A., Horvath A., Doczi T., Bogner P., Janszky J. Comparison of accuracy between FSL's FIRST and Freesurfer for caudate nucleus and putamen segmentation. ESMRMB Congress (2015.10.01-03.). Edinburgh, UK, (Poster and oral presentation)

Orsi G., Perlaki G., Horvath R., **Nagy S.A.**, Horvath A., Bogner P., Janszky J. Comparison of accuracy between FSL's FIRST and Freesurfer for caudate nucleus and putamen segmentation. Neuroimaging workshop (2015.04.17-18.). Szeged, Hungary

Hetenyi Sz., **Nagy S.A.**, Horvath F., Toth K., Vaczi M., Illes Zs., Bogner P. Volumetric changes of hamstring muscles after exercise in patients with Pompe disease. European Society of Musculoskeletal Radiology (2015.06.18-20.). York, UK. (Poster presentation)

Horvath A., Perlaki G., Toth A., Orsi G., **Nagy S.A.**, Doczi T., Horvath Zs., Bogner P. Diffusion alterations in the normal appearing white matter of glioma and meningioma patients. Neuroimaging workshop (2015.04.17-18.). Szeged, Hungary

Hajnal A., **Nagy S.A.** Funkcionális MRI vizsgálatok a rutin diagnosztikában. A Magyar Radiológus Asszisztensek Egyesületének XVIII. Kongresszusa (2014.09.25-27.). Kaposvár, Hungary

Perlaki G., Orsi G., **Nagy S.A.**, Bogner P., Bihari K., Bone B., Acs P., Komoly S., Aschermann Zs. Quantitative MRI of iron deposition in cervical dystonia. A Magyar Neuroradiológiai Társaság XXII. Kongresszusa (2014.11.06-08.). Hajduszoboszló, Hungary

Horvath A., **Nagy S.A.**, Perlaki G., Orsi G., Toth A., Doczi T., Horvath Zs., Bogner P. Diffusion signal changes in normal appearing white matter of glioma patients. A Magyar Neuroradiológiai Társaság XXII. Kongresszusa (2014.11.06-08.). Hajduszoboszló, Hungary

Horvath A., **Nagy S.A.**, Perlaki G., Orsi G., Toth A., Bogner P., Doczi T. Multimodal quantitative characterization of intracranial epidermoid cysts: preliminary results. Hungarian Medical Association of America: 7th Balatonfüred Meeting (2014.08.22-23.). Balatonfüred, Hungary

Nagy S.A. MR imaging in Pompe disease. Annual Hungarian Pompe meeting (2014.08.21-22.). Siófok, Hungary

Horvath A., **Nagy S.A.**, Perlaki G., Orsi G., Toth A., Horvath Zs., Doczi T., Bogner P. New trends in perfusion MRI. Neuroimaging workshop (2014.04.25-26.). Debrecen, Hungary

Horvath A., **Nagy S.A.**, Perlaki G., Toth A., Orsi G., Aradi M., Komaromy H., Doczi T., Bogner P. A quantitative approach in characterization of epidermoid cyst and middle ear cholesteatoma: T1 and T2 mapping. European Congress of Radiology (2014.03.06-10.). Vienna, Austria (Electronic poster)

Horvath A., **Nagy S.A.**, Perlaki G., Orsi G., Aradi M., Horvath Zs., Bogner P. Perfusion MRI methods in different neoplasms. A Magyar Neuroradiológiai Társaság XXI. Kongresszusa (2013.11.07-09.). Visegrád, Hungary

Perlaki G., Orsi G., **Nagy S.A.**, Horvath R., Moricz P., Schwarcz A., Bogner P., Janszky J. Olfactory fMRI: Initial results. A Magyar Neuroradiológiai Társaság XXI. Kongresszusa (2013.11.07-09.). Visegrád, Hungary

Orsi G., Aradi M., **Nagy S.A.**, Bogner P., Janszky J., Illes Zs., Perlaki G., Doczi T., Pfund Z., Schwarcz A. Biexponential diffusion signal changes in migraine and multiple sclerosis. A Magyar Neuroradiológiai Társaság XXI. Kongresszusa (2013.11.07-09.). Visegrád, Hungary

Orsi G., Aradi M., **Nagy S.A.**, Perlaki G., Trauninger A., Bogner P., Janszky J., Illes Zs., Doczi T., Pfund Z., Schwarcz A. Differentiating White Matter Lesions in Multiple Sclerosis and Migraine Using Monoexponential and Biexponential Diffusion Measurements. ISMRM Scientific Workshop (2013.10.14-18.). Podstrana, Croatia (Poster presentation)

Vaczi M., Bogner P., Koszegi T., Ambrus M., **Nagy S.A.**, Perlaki G., Orsi G., Toth K., Hortobagyi T. Rapid stretching of the activated ageing muscle induces favourable mechanical, morphometric and hormonal change. 18th Annual Congress of the European College of Sport Science (2013.06.26-29.). Barcelona, Spain

Vaczi M., Bogner P., Koszegi T., Ambrus M., **Nagy S.A.**, Perlaki G., Orsi G., Toth K., Hortobagyi T., Bartusne Szmodis M. Nyújtásos-rövidüléses és excentrikus edzés kedvező mechanikai, morfometriai és hormonális hatása az öregedő izomban. X. Országos Sporttudományi Kongresszus (2013.05.29-30.). Nyíregyháza, Hungary

Toth A., Szijjarto G., Perlaki G., **Nagy S.A.**, Orsi G., Schwarcz A., Pal J. Dark cells appearance in Mild and Acute Traumatic Brain Injury of rats: A magnetic resonance imaging study. Neuroimaging Workshop (2013.04.19-20.). Pécs, Hungary

Plozer E., Altbäcker A., Darnai G., Perlaki G., Osri G., **Nagy S.A.**, Koszegi T., Schwarcz A., Komoly S., Janszky J., Clemens Zs. Intracranial volume inversely correlates with serum 25(OH)D level in healthy young women. Neuroimaging Workshop (2013.04.19-20.). Pécs, Hungary

Perlaki G., Osri G., **Nagy S.A.**, Plozer E., Altbäcker A., Darnai G., Toth A., Doczi T., Komoly S., Bogner P., Schwarcz A., Janszky J. Are there any gender differences in the hippocampus volume after head-size correction? A volumetric and voxel-based morphometric study. Neuroimaging Workshop (2013.04.19-20.). Pécs, Hungary

Altbäcker A., Plozer E., Darnai G., Perlaki G., Orsi G., **Nagy S.A.**, Schwarcz A., Clemens Zs., Janszky J. Problematic internet use is associated with structural alterations in the brain: Preliminary results. Neuroimaging Workshop (2013.04.19-20.). Pécs, Hungary

Orsi G., Aradi M., **Nagy S.A.**, Plozer E., Bogner P., Janszky J., Illes Zs., Perlaki G., Doczi T., Pfund Z., Schwarcz A. Bi-exponential diffusion signal decay in migraine and multiple sclerosis. A Magyar Neuroradiológiai Társaság XX. Kongresszusa (2012.11.08-10.). Eger, Hungary

Dervali M., **Nagy S.A.**, Bogner P., Vaczi M., Perlaki G., Orsi G., Aradi M. A combhajlító izmok kvantitatív MRvizsgálata: a terhelés hatásának monitorozása. A Magyar Radiológus Asszisztensek Egyesületének XVII. Kongresszusa (2012.10.11-13.). Miskolc, Hungary

Lehmann B., Bogner P., **Nagy S.A.**, Somogyi G., Lehmann Be., Dervali M., Reisch O., Aradi M., Perlaki G., Vancsodi J., Bardos T., Hetenyi Sz. Hyalinporc kvantitatív MR-vizsgálata processzált porc-allograft transzplantációját követően. A Magyar Radiológus Asszisztensek Egyesületének XVII. Kongresszusa (2012.10.11-13.). Miskolc, Hungary

Lehmann Be., Bogner P., Imre M., **Nagy S.A.**, Lehmann B., Reisch O., Dervali M. Az MR enterográfia legújabb aspektusai Magyarországon. A Magyar Radiológus Asszisztensek Egyesületének XVII. Kongresszusa (2012.10.11-13.). Miskolc, Hungary

Horvath A., **Nagy S.A.**, Bogner P., Aradi M., Orsi G., Perlaki G., Komaromy H., Schwarcz A., Janszky J. Quantitative MR imaging of cholesteatoma with T1 and T2 mapping. Hungarian Medical Association of America: 6th Balatonfüred Meeting (2012.08.18-19.). Balatonfüred, Hungary

Nagy S.A., Bogner P., Vaczi M., Perlaki G., Orsi G., Aradi M. A combhajlító izmok kvantitatív MR vizsgálata: a terhelés hatásának monitorozása. A Magyar Radiológusok Társasága XXVI. Kongresszusa (2012. 06. 21-23.). Debrecen, Hungary

Bogner P., **Nagy S.A.**, Somogyi G., Aradi M., Perlaki G., Vancsodi J., Bardos T., Hetenyi Sz. Hyalinporc kvantitatív MR-vizsgálata processzált porc-allograft transzplantációját követően. A Magyar Radiológusok Társasága XXVI. Kongresszusa (2012. 06. 21-23.). Debrecen, Hungary

11. References

Adams M.A., Roughley P.J. What is intervertebral disc degeneration, and what causes it? ***(2006)***. Spine (Phila Pa 1976) 31:2151-61.

Ahmadi M.E., Hagler D.J., Jr., McDonald C.R., Tecoma E.S., Iragui V.J., Dale A.M., Halgren E. Side matters: diffusion tensor imaging tractography in left and right temporal lobe epilepsy (2009). AJNR Am J Neuroradiol 30:1740-7.

Alajbegovic A., Loga N., Tiro N., Alajbegovic S., Cindro V., Hozo I. Cognitive and depressive disorders in multiple sclerosis (2009). Acta Clin Croat 48:3-8.

Andersson J., Jenkinson M., Smith S. (2007) Non-linear registration aka Spatial normalisation FMRIB Technial Report TR07JA2, FMRIB Centre, Oxford, United Kingdom. pp. 1-21.

Aprill C., Bogduk N. High-intensity zone: a diagnostic sign of painful lumbar disc on magnetic resonance imaging (1992). Br J Radiol 65:361-9.

Arana E., Royuela A., Kovacs F.M., Estremera A., Sarasibar H., Amengual G., Galarraga I., Martinez C., Muriel A., Abraira V., Gil Del Real M.T., Zamora J., Campillo C. Lumbar spine: agreement in the interpretation of 1.5-T MR images by using the Nordic Modic Consensus Group classification form (2010). Radiology 254:809-17.

Armspach J.P., Gounot D., Rumbach L., Chambron J. In vivo determination of multiexponential T2 relaxation in the brain of patients with multiple sclerosis (1991). Magn Reson Imaging 9:107-13.

Assaf Y., Cohen Y. Non-mono-exponential attenuation of water and N-acetyl aspartate signals due to diffusion in brain tissue (1998). J Magn Reson 131:69-85.

Bakshi R., Thompson A.J., Rocca M.A., Pelletier D., Dousset V., Barkhof F., Inglese M., Guttmann C.R., Horsfield M.A., Filippi M. MRI in multiple sclerosis: current status and future prospects (2008). Lancet Neurol 7:615-25.

Baldwin G.N., Tsuruda J.S., Maravilla K.R., Hamill G.S., Hayes C.E. The fornix in patients with seizures caused by unilateral hippocampal sclerosis: detection of unilateral volume loss on MR images (1994). AJR Am J Roentgenol 162:1185-9.

Barkovich A.J. Concepts of myelin and myelination in neuroradiology (2000). AJNR Am J Neuroradiol 21:1099-109.

Bastin M.E., Sinha S., Whittle I.R., Wardlaw J.M. Measurements of water diffusion and T1 values in peritumoural oedematous brain (2002). Neuroreport 13:1335-40.

Beattie P.F., Morgan P.S., Peters D. Diffusion-weighted magnetic resonance imaging of normal and degenerative lumbar intervertebral discs: a new method to potentially quantify the physiologic effect of physical therapy intervention (2008). J Orthop Sports Phys Ther 38:42-9.

Beaulieu C., Fenrich F.R., Allen P.S. Multicomponent water proton transverse relaxation and T2-discriminated water diffusion in myelinated and nonmyelinated nerve (1998). Magn Reson Imaging 16:1201-10.

Bernasconi N., Natsume J., Bernasconi A. Progression in temporal lobe epilepsy: differential atrophy in mesial temporal structures (2005). Neurology 65:223-8.

Birkfellner W. (2011) Applied medical image processing : a basic course Taylor & Francis, Boca Raton.

Burgmans S., van Boxtel M.P., Gronenschild E.H., Vuurman E.F., Hofman P., Uylings H.B., Jolles J., Raz N. Multiple indicators of age-related differences in cerebral white matter and the modifying effects of hypertension (2010). Neuroimage 49:2083-93.

Camara E., Bodammer N., Rodriguez-Fornells A., Tempelmann C. Age-related water diffusion changes in human brain: a voxel-based approach (2007). Neuroimage 34:1588-99.

Caramia F., Pantano P., Di Legge S., Piattella M.C., Lenzi D., Paolillo A., Nucciarelli W., Lenzi G.L., Bozzao L., Pozzilli C. A longitudinal study of MR diffusion changes in normal appearing white matter of patients with early multiple sclerosis (2002). Magn Reson Imaging 20:383-8.

Carrino J.A., Lurie J.D., Tosteson A.N., Tosteson T.D., Carragee E.J., Kaiser J., Grove M.R., Blood E., Pearson L.H., Weinstein J.N., Herzog R. Lumbar spine: reliability of MR imaging findings (2009). Radiology 250:161-70.

Cendes F., Leproux F., Melanson D., Ethier R., Evans A., Peters T., Andermann F. MRI of amygdala and hippocampus in temporal lobe epilepsy (1993). J Comput Assist Tomogr 17:206-10.

Chan Y.H. Biostatistics 201: linear regression analysis (2004). Singapore Med J 45:55-61.

Claudia C., Farida C., Guy G., Marie-Claude M., Carl-Eric A. Quantitative evaluation of an automatic segmentation method for 3D reconstruction of intervertebral scoliotic disks from MR images (2012). BMC Med Imaging 12:26.

Cohen-Adad J., Wheeler-Kingshott C.A.M. (2014) Quantitative MRI of the spinal cord Elsevier/Academic Press, Amsterdam ; Boston.

Cohen O.S., Hoffmann C., Lee H., Chapman J., Fulbright R.K., Prohovnik I. MRI detection of the cerebellar syndrome in Creutzfeldt-Jakob disease (2009). Cerebellum 8:373-81.

Collins D.L., Neelin P., Peters T.M., Evans A.C. Automatic 3D intersubject registration of MR volumetric data in standardized Talairach space (1994). J Comput Assist Tomogr 18:192-205.

Concha L., Beaulieu C., Collins D.L., Gross D.W. White-matter diffusion abnormalities in temporal-lobe epilepsy with and without mesial temporal sclerosis (2009). J Neurol Neurosurg Psychiatry 80:312-9.

Concha L., Beaulieu C., Gross D.W. Bilateral limbic diffusion abnormalities in unilateral temporal lobe epilepsy (2005). Ann Neurol 57:188-96.

de Carvalho Rangel C., Hygino Cruz L.C., Jr., Takayassu T.C., Gasparetto E.L., Domingues R.C. Diffusion MR imaging in central nervous system (2011). Magn Reson Imaging Clin N Am 19:23-53.

de Schepper E.I., Damen J., van Meurs J.B., Ginai A.Z., Popham M., Hofman A., Koes B.W., Bierma-Zeinstra S.M. The association between lumbar disc degeneration and low back pain: the influence of age, gender, and individual radiographic features (2010). Spine (Phila Pa 1976) 35:531-6.

DeLano M.C., Cooper T.G., Siebert J.E., Potchen M.J., Kuppusamy K. High-b-value diffusion-weighted MR imaging of adult brain: image contrast and apparent diffusion coefficient map features (2000). AJNR Am J Neuroradiol 21:1830-6.

Diehl B., Busch R.M., Duncan J.S., Piao Z., Tkach J., Luders H.O. Abnormalities in diffusion tensor imaging of the uncinate fasciculus relate to reduced memory in temporal lobe epilepsy (2008). Epilepsia 49:1409-18.

Ellingson A.M., Mehta H., Polly D.W., Ellermann J., Nuckley D.J. Disc degeneration assessed by quantitative T2* (T2 star) correlated with functional lumbar mechanics (2013). Spine (Phila Pa 1976) 38:E1533-40.

Fardon D.F., Milette P.C., Combined Task Forces of the North American Spine Society A.S.o.S.R., American Society of N. Nomenclature and classification of lumbar disc pathology. Recommendations of the Combined task Forces of the North American Spine Society, American Society of Spine Radiology, and American Society of Neuroradiology (2001). Spine (Phila Pa 1976) 26:E93-E113.

Fazekas F., Ropele S., Enzinger C., Gorani F., Seewann A., Petrovic K., Schmidt R. MTI of white matter hyperintensities (2005). Brain 128:2926-32.

Filippi M., Rocca M.A. MRI evidence for multiple sclerosis as a diffuse disease of the central nervous system (2005). J Neurol 252 Suppl 5:v16-24.

Filippi M., Rocca M.A., Horsfield M.A., Hametner S., Geurts J.J., Comi G., Lassmann H. Imaging cortical damage and dysfunction in multiple sclerosis (2013). JAMA Neurol 70:556-64.

Fischl B., Salat D.H., Busa E., Albert M., Dieterich M., Haselgrove C., van der Kouwe A., Killiany R., Kennedy D., Klaveness S., Montillo A., Makris N., Rosen B., Dale A.M. Whole brain segmentation: automated labeling of neuroanatomical structures in the human brain (2002). Neuron 33:341-55.

Fischl B., Salat D.H., van der Kouwe A.J., Makris N., Segonne F., Quinn B.T., Dale A.M. Sequence-independent segmentation of magnetic resonance images (2004). Neuroimage 23 Suppl 1:S69-84.

Flugel D., Cercignani M., Symms M.R., O'Toole A., Thompson P.J., Koepp M.J., Foong J. Diffusion tensor imaging findings and their correlation with neuropsychological deficits in patients with temporal lobe epilepsy and interictal psychosis (2006). Epilepsia 47:941-4.

Focke N.K., Yogarajah M., Bonelli S.B., Bartlett P.A., Symms M.R., Duncan J.S. Voxel-based diffusion tensor imaging in patients with mesial temporal lobe epilepsy and hippocampal sclerosis (2008). Neuroimage 40:728-37.

Forbes K.P., Pipe J.G., Bird C.R. Changes in brain water diffusion during the 1st year of life (2002). Radiology 222:405-9.

Francis P.L., Jakubovic R., O'Connor P., Zhang L., Eilaghi A., Lee L., Carroll T.J., Mouannes-Srour J., Feinstein A., Aviv R.I. Robust perfusion deficits in cognitively impaired patients with secondary-progressive multiple sclerosis (2013). AJNR Am J Neuroradiol 34:62-7.

Garaci F.G., Colangelo V., Ludovici A., Gaudiello F., Marziali S., Centonze D., Boffa L., Simonetti G., Floris R. A diffusion longitudinal MR imaging study in normal-appearing white matter in untreated relapsing-remitting multiple sclerosis (2007). AJNR Am J Neuroradiol 28:475-8.

Garaci F.G., Floris R., Bozzao A., Manenti G., Simonetti A., Lupattelli T., Curatolo P., Simonetti G. Increased brain apparent diffusion coefficient in tuberous sclerosis (2004). Radiology 232:461-5.

Gillard J.H., Waldman A.D., Barker P.B. (2009) Clinical MR Neuroimaging: Physiological and Functional Techniques 2nd Edition Cambridge University Press.

Griffith J.F., Wang Y.X., Antonio G.E., Choi K.C., Yu A., Ahuja A.T., Leung P.C. Modified Pfirrmann grading system for lumbar intervertebral disc degeneration (2007). Spine (Phila Pa 1976) 32:E708-12.

Gross D.W., Concha L., Beaulieu C. Extratemporal white matter abnormalities in mesial temporal lobe epilepsy demonstrated with diffusion tensor imaging (2006). Epilepsia 47:1360-3.

Gunzburg R., Parkinson R., Moore R., Cantraine F., Hutton W., Vernon-Roberts B., Fraser R. A cadaveric study comparing discography, magnetic resonance imaging, histology, and mechanical behavior of the human lumbar disc (1992). Spine (Phila Pa 1976) 17:417-26.

Haneder S., Apprich S.R., Schmitt B., Michaely H.J., Schoenberg S.O., Friedrich K.M., Trattnig S. Assessment of glycosaminoglycan content in intervertebral discs using chemical exchange saturation transfer at 3.0 Tesla: preliminary results in patients with low-back pain (2013). Eur Radiol 23:861-8.

Hangai M., Kaneoka K., Hinotsu S., Shimizu K., Okubo Y., Miyakawa S., Mukai N., Sakane M., Ochiai N. Lumbar intervertebral disk degeneration in athletes (2009). Am J Sports Med 37:149-55.

Hanyu H., Shindo H., Kakizaki D., Abe K., Iwamoto T., Takasaki M. Increased water diffusion in cerebral white matter in Alzheimer's disease (1997). Gerontology 43:343-51.

Hermann B., Seidenberg M., Bell B., Rutecki P., Sheth R., Ruggles K., Wendt G., O'Leary D., Magnotta V. The neurodevelopmental impact of childhood-onset temporal lobe epilepsy on brain structure and function (2002). Epilepsia 43:1062-71.

Horvath A., Perlaki G., Toth A., Orsi G., Nagy S., Doczi T., Horvath Z., Bogner P. Biexponential diffusion alterations in the normal-appearing white matter of glioma patients might indicate the presence of global vasogenic edema (2016a). J Magn Reson Imaging 44:633-41.

Horvath A., Perlaki G., Toth A., Orsi G., Nagy S., Doczi T., Horvath Z., Bogner P. Increased diffusion in the normal appearing white matter of brain tumor patients: is this just tumor infiltration? (2016b). J Neurooncol 127:83-90.

Hwang D., Kim S., Abeydeera N.A., Statum S., Masuda K., Chung C.B., Siriwanarangsun P., Bae W.C. Quantitative magnetic resonance imaging of the lumbar intervertebral discs (2016). Quant Imaging Med Surg 6:744-755.

Janszky J., Janszky I., Ebner A. Age at onset in mesial temporal lobe epilepsy with a history of febrile seizures (2004). Neurology 63:1296-8.

Jazini E., Sharan A.D., Morse L.J., Dyke J.P., Aronowitz E.B., Chen L.K., Tang S.Y. Alterations in T2 relaxation magnetic resonance imaging of the ovine intervertebral disc due to nonenzymatic glycation (2012). Spine (Phila Pa 1976) 37:E209-15.

Jenkins J.P., Hickey D.S., Zhu X.P., Machin M., Isherwood I. MR imaging of the intervertebral disc: a quantitative study (1985). Br J Radiol 58:705-9.

Jenkinson M., Smith S. A global optimisation method for robust affine registration of brain images (2001). Med Image Anal 5:143-56.

Johannessen W., Auerbach J.D., Wheaton A.J., Kurji A., Borthakur A., Reddy R., Elliott D.M. Assessment of human disc degeneration and proteoglycan content using T1rho-weighted magnetic resonance imaging (2006). Spine (Phila Pa 1976) 31:1253-7.

Jones R.A., Palasis S., Grattan-Smith J.D. The evolution of the apparent diffusion coefficient in the pediatric brain at low and high diffusion weightings (2003). J Magn Reson Imaging 18:665-74.

Kanayama M., Togawa D., Takahashi C., Terai T., Hashimoto T. Cross-sectional magnetic resonance imaging study of lumbar disc degeneration in 200 healthy individuals (2009). J Neurosurg Spine 11:501-7.

Kanzow C., Yamashita N., Fukushima M. Levenberg–Marquardt methods with strong local convergence properties for solving nonlinear equations with convex constraints (2004). Journal of Computational and Applied Mathematics 172:375-397.

Kemmotsu N., Girard H.M., Bernhardt B.C., Bonilha L., Lin J.J., Tecoma E.S., Iragui V.J., Hagler D.J., Jr., Halgren E., McDonald C.R. MRI analysis in temporal lobe epilepsy: cortical thinning and white matter disruptions are related to side of seizure onset (2011). Epilepsia 52:2257-66.

Kettler A., Wilke H.J. Review of existing grading systems for cervical or lumbar disc and facet joint degeneration (2006). Eur Spine J 15:705-18.

Kiferle L., Politis M., Muraro P.A., Piccini P. Positron emission tomography imaging in multiple sclerosis-current status and future applications (2011). Eur J Neurol 18:226-31.

Kim H., Piao Z., Liu P., Bingaman W., Diehl B. Secondary white matter degeneration of the corpus callosum in patients with intractable temporal lobe epilepsy: a diffusion tensor imaging study (2008). Epilepsy Res 81:136-42.

Kundu A. Local segmentation of biomedical images (1990). Comput Med Imaging Graph 14:173-83.

Kurtzke J.F. Rating neurologic impairment in multiple sclerosis: an expanded disability status scale (EDSS) (1983). Neurology 33:1444-52.

Landis J.R., Koch G.G. The measurement of observer agreement for categorical data (1977). Biometrics 33:159-74.

Lawson C.L., Hanson R.J. (1995) Solving least squares problems SIAM, Philadelphia.

Le Bihan D., van Zijl P. From the diffusion coefficient to the diffusion tensor (2002). NMR Biomed 15:431-4.

Lebel R.M., Wilman A.H. Transverse relaxometry with stimulated echo compensation (2010). Magn Reson Med 64:1005-14.

Lee D.Y., Fletcher E., Martinez O., Ortega M., Zozulya N., Kim J., Tran J., Buonocore M., Carmichael O., DeCarli C. Regional pattern of white matter microstructural changes in normal aging, MCI, and AD (2009). Neurology 73:1722-8.

Li Y., Jewells V., Kim M., Chen Y., Moon A., Armao D., Troiani L., Markovic-Plese S., Lin W., Shen D. Diffusion tensor imaging based network analysis detects alterations of neuroconnectivity in patients with clinically early relapsing-remitting multiple sclerosis (2013). Hum Brain Mapp 34:3376-91.

Lin J.J., Riley J.D., Juranek J., Cramer S.C. Vulnerability of the frontal-temporal connections in temporal lobe epilepsy (2008). Epilepsy Res 82:162-70.

Liu Y., Soppi V., Mustonen T., Kononen M., Koivisto T., Koskela A., Rinne J., Vanninen R.L. Subarachnoid hemorrhage in the subacute stage: elevated apparent diffusion coefficient in normal-appearing brain tissue after treatment (2007). Radiology 242:518-25.

Lurie J.D., Tosteson A.N., Tosteson T.D., Carragee E., Carrino J.A., Kaiser J., Sequeiros R.T., Lecomte A.R., Grove M.R., Blood E.A., Pearson L.H., Herzog R., Weinstein J.N. Reliability of magnetic resonance imaging readings for lumbar disc herniation in the Spine Patient Outcomes Research Trial (SPORT) (2008). Spine (Phila Pa 1976) 33:991-8.

MacKay A., Whittall K., Adler J., Li D., Paty D., Graeb D. In vivo visualization of myelin water in brain by magnetic resonance (1994). Magn Reson Med 31:673-7.

Maier C.F., Tan S.G., Hariharan H., Potter H.G. T2 quantitation of articular cartilage at 1.5 T (2003). J Magn Reson Imaging 17:358-64.

Maier S.E., Sun Y., Mulkern R.V. Diffusion imaging of brain tumors (2010). NMR Biomed 23:849-64.

Maier S.E., Vajapeyam S., Mamata H., Westin C.F., Jolesz F.A., Mulkern R.V. Biexponential diffusion tensor analysis of human brain diffusion data (2004). Magn Reson Med 51:321-30.

Majumdar S., Orphanoudakis S.C., Gmitro A., O'Donnell M., Gore J.C. Errors in the measurements of T2 using multiple-echo MRI techniques. II. Effects of static field inhomogeneity (1986). Magn Reson Med 3:562-74.

Malone M.J., Szoke M.C. Neurochemical studies in aging brain. I. Structural changes in myelin lipids (1982). J Gerontol 37:262-7.

Mamourian A.C., Brown D.B. Asymmetric mamillary bodies: MR identification (1993). AJNR Am J Neuroradiol 14:1332-5; discussion 1336-42.

Marinelli N.L., Haughton V.M., Anderson P.A. T2 relaxation times correlated with stage of lumbar intervertebral disk degeneration and patient age (2010). AJNR Am J Neuroradiol 31:1278-82.

Marinelli N.L., Haughton V.M., Munoz A., Anderson P.A. T2 relaxation times of intervertebral disc tissue correlated with water content and proteoglycan content (2009). Spine (Phila Pa 1976) 34:520-4.

Marner L., Nyengaard J.R., Tang Y., Pakkenberg B. Marked loss of myelinated nerve fibers in the human brain with age (2003). J Comp Neurol 462:144-52.

McDonald C.R., Hagler D.J., Jr., Ahmadi M.E., Tecoma E., Iragui V., Gharapetian L., Dale A.M., Halgren E. Regional neocortical thinning in mesial temporal lobe epilepsy (2008). Epilepsia 49:794-803.

Meier D.S., Weiner H.L., Guttmann C.R. MR imaging intensity modeling of damage and repair in multiple sclerosis: relationship of short-term lesion recovery to progression and disability (2007). AJNR Am J Neuroradiol 28:1956-63.

Milford D., Rosbach N., Bendszus M., Heiland S. Mono-Exponential Fitting in T2-Relaxometry: Relevance of Offset and First Echo (2015). PLoS One 10:e0145255.

Miller D.H., Barkhof F., Frank J.A., Parker G.J., Thompson A.J. Measurement of atrophy in multiple sclerosis: pathological basis, methodological aspects and clinical relevance (2002). Brain 125:1676-95.

Miller D.H., Thompson A.J., Filippi M. Magnetic resonance studies of abnormalities in the normal appearing white matter and grey matter in multiple sclerosis (2003). J Neurol 250:1407-19.

Milne M.L., Conradi M.S. Multi-exponential signal decay from diffusion in a single compartment (2009). J Magn Reson 197:87-90.

Modic M.T., Steinberg P.M., Ross J.S., Masaryk T.J., Carter J.R. Degenerative disk disease: assessment of changes in vertebral body marrow with MR imaging (1988). Radiology 166:193-9.

Moore G.R., Laule C., Mackay A., Leung E., Li D.K., Zhao G., Traboulsee A.L., Paty D.W. Dirty-appearing white matter in multiple sclerosis: preliminary observations of myelin phospholipid and axonal loss (2008). J Neurol 255:1802-11.

Mulkern R.V., Vajapeyam S., Robertson R.L., Caruso P.A., Rivkin M.J., Maier S.E. Biexponential apparent diffusion coefficient parametrization in adult vs newborn brain (2001). Magn Reson Imaging 19:659-68.

Mulkern R.V., Wong S.T., Jakab P., Bleier A.R., Sandor T., Jolesz F.A. CPMG imaging sequences for high field in vivo transverse relaxation studies (1990). Magn Reson Med 16:67-79.

Naganawa S., Sato K., Katagiri T., Mimura T., Ishigaki T. Regional ADC values of the normal brain: differences due to age, gender, and laterality (2003). Eur Radiol 13:6-11.

Nguyen A.M., Johannessen W., Yoder J.H., Wheaton A.J., Vresilovic E.J., Borthakur A., Elliott D.M. Noninvasive quantification of human nucleus pulposus pressure with use of T1rho-weighted magnetic resonance imaging (2008). J Bone Joint Surg Am 90:796-802.

Niendorf T., Dijkhuizen R.M., Norris D.G., van Lookeren Campagne M., Nicolay K. Biexponential diffusion attenuation in various states of brain tissue: implications for diffusion-weighted imaging (1996). Magn Reson Med 36:847-57.

Niinimaki J., Korkiakoski A., Ojala O., Karppinen J., Ruohonen J., Haapea M., Korpelainen R., Natri A., Tervonen O. Association between visual degeneration of intervertebral discs and the apparent diffusion coefficient (2009). Magn Reson Imaging 27:641-7.

Niu G., Yang J., Wang R., Dang S., Wu E.X., Guo Y. MR imaging assessment of lumbar intervertebral disk degeneration and age-related changes: apparent diffusion coefficient versus T2 quantitation (2011). AJNR Am J Neuroradiol 32:1617-23.

Norris D.G. The effects of microscopic tissue parameters on the diffusion weighted magnetic resonance imaging experiment (2001). NMR Biomed 14:77-93.

Oishi K., Faria A., Van Zijl P., Mori S. (2010) MRI Atlas of Human White Matter 2nd Edition Academic Press.

Otte W.M., van Eijsden P., Sander J.W., Duncan J.S., Dijkhuizen R.M., Braun K.P. A meta-analysis of white matter changes in temporal lobe epilepsy as studied with diffusion tensor imaging (2012). Epilepsia 53:659-67.

Paajanen H., Komu M., Lehto I., Laato M., Haapasalo H. Magnetization transfer imaging of lumbar disc degeneration. Correlation of relaxation parameters with biochemistry (1994). Spine (Phila Pa 1976) 19:2833-7.

Perry J., Haughton V., Anderson P.A., Wu Y., Fine J., Mistretta C. The value of T2 relaxation times to characterize lumbar intervertebral disks: preliminary results (2006). AJNR Am J Neuroradiol 27:337-42.

Pfirrmann C.W., Metzdorf A., Zanetti M., Hodler J., Boos N. Magnetic resonance classification of lumbar intervertebral disc degeneration (2001). Spine (Phila Pa 1976) 26:1873-8.

Powell H.W., Parker G.J., Alexander D.C., Symms M.R., Boulby P.A., Wheeler-Kingshott C.A., Barker G.J., Koepp M.J., Duncan J.S. Abnormalities of language networks in temporal lobe epilepsy (2007). Neuroimage 36:209-21.

Pye S.R., Reid D.M., Lunt M., Adams J.E., Silman A.J., O'Neill T.W. Lumbar disc degeneration: association between osteophytes, end-plate sclerosis and disc space narrowing (2007). Ann Rheum Dis 66:330-3.

Pye S.R., Reid D.M., Smith R., Adams J.E., Nelson K., Silman A.J., O'Neill T.W. Radiographic features of lumbar disc degeneration and self-reported back pain (2004). J Rheumatol 31:753-8.

Riley J.D., Franklin D.L., Choi V., Kim R.C., Binder D.K., Cramer S.C., Lin J.J. Altered white matter integrity in temporal lobe epilepsy: association with cognitive and clinical profiles (2010). Epilepsia 51:536-45.

Rodrigo S., Oppenheim C., Chassoux F., Golestani N., Cointepas Y., Poupon C., Semah F., Mangin J.F., Le Bihan D., Meder J.F. Uncinate fasciculus fiber tracking in mesial temporal lobe epilepsy. Initial findings (2007). Eur Radiol 17:1663-8.

Rohde G.K., Barnett A.S., Basser P.J., Marenco S., Pierpaoli C. Comprehensive approach for correction of motion and distortion in diffusion-weighted MRI (2004). Magn Reson Med 51:103-14.

Sacerdoti F.M., Giordano A., SpringerLink (Online service). (2016) Advanced Imaging Techniques in Clinical Pathology Springer New York : Imprint: Humana Press, New York, NY.

Sala S., Agosta F., Pagani E., Copetti M., Comi G., Filippi M. Microstructural changes and atrophy in brain white matter tracts with aging (2012). Neurobiol Aging 33:488-498 e2.

Sayin U., Hutchinson E., Meyerand M.E., Sutula T. Age-dependent long-term structural and functional effects of early-life seizures: evidence for a hippocampal critical period influencing plasticity in adulthood (2015). Neuroscience 288:120-34.

Scanlon C., Mueller S.G., Cheong I., Hartig M., Weiner M.W., Laxer K.D. Grey and white matter abnormalities in temporal lobe epilepsy with and without mesial temporal sclerosis (2013). J Neurol 260:2320-9.

Scherfler C., Schocke M.F., Seppi K., Esterhammer R., Brenneis C., Jaschke W., Wenning G.K., Poewe W. Voxel-wise analysis of diffusion weighted imaging reveals disruption of the olfactory tract in Parkinson's disease (2006). Brain 129:538-42.

Schleich C., Muller-Lutz A., Eichner M., Schmitt B., Matuschke F., Bittersohl B., Zilkens C., Wittsack H.J., Antoch G., Miese F. Glycosaminoglycan Chemical Exchange Saturation Transfer of Lumbar Intervertebral Discs in Healthy Volunteers (2016). Spine (Phila Pa 1976) 41:146-52.

Schmidt R., Ropele S., Ferro J., Madureira S., Verdelho A., Petrovic K., Gouw A., van der Flier W.M., Enzinger C., Pantoni L., Inzitari D., Erkinjuntti T., Scheltens P., Wahlund L.O., Waldemar G., Rostrup E., Wallin A., Barkhof F., Fazekas F. Diffusion-weighted imaging and cognition in the leukoariosis and disability in the elderly study (2010). Stroke 41:e402-8.

Schmierer K., Altmann D.R., Kassim N., Kitzler H., Kerskens C.M., Doege C.A., Aktas O., Lunemann J.D., Miller D.H., Zipp F., Villringer A. Progressive change in primary progressive multiple sclerosis normal-appearing white matter: a serial diffusion magnetic resonance imaging study (2004). Mult Scler 10:182-7.

Schneiderman G., Flannigan B., Kingston S., Thomas J., Dillin W.H., Watkins R.G. Magnetic resonance imaging in the diagnosis of disc degeneration: correlation with discography (1987). Spine (Phila Pa 1976) 12:276-81.

Segonne F., Dale A.M., Busa E., Glessner M., Salat D., Hahn H.K., Fischl B. A hybrid approach to the skull stripping problem in MRI (2004). Neuroimage 22:1060-75.

Seidenberg M., Kelly K.G., Parrish J., Geary E., Dow C., Rutecki P., Hermann B. Ipsilateral and contralateral MRI volumetric abnormalities in chronic unilateral temporal lobe epilepsy and their clinical correlates (2005). Epilepsia 46:420-30.

Sim J., Wright C.C. The kappa statistic in reliability studies: use, interpretation, and sample size requirements (2005). Phys Ther 85:257-68.

Sled J.G., Zijdenbos A.P., Evans A.C. A nonparametric method for automatic correction of intensity nonuniformity in MRI data (1998). IEEE Trans Med Imaging 17:87-97.

Smith S.M. Fast robust automated brain extraction (2002). Hum Brain Mapp 17:143-55.

Smith S.M., Jenkinson M., Johansen-Berg H., Rueckert D., Nichols T.E., Mackay C.E., Watkins K.E., Ciccarelli O., Cader M.Z., Matthews P.M., Behrens T.E. Tract-based spatial statistics: voxelwise analysis of multi-subject diffusion data (2006). Neuroimage 31:1487-505.

Stelzeneder D., Welsch G.H., Kovacs B.K., Goed S., Paternostro-Sluga T., Vlychou M., Friedrich K., Mamisch T.C., Trattnig S. Quantitative T2 evaluation at 3.0T compared to morphological grading of the lumbar intervertebral disc: a standardized evaluation approach in patients with low back pain (2012). Eur J Radiol 81:324-30.

Sukstanskii A.L., Ackerman J.J., Yablonskiy D.A. Effects of barrier-induced nuclear spin magnetization inhomogeneities on diffusion-attenuated MR signal (2003). Magn Reson Med 50:735-42.

Suzuki M., Hagino H., Nohara S., Zhou S.Y., Kawasaki Y., Takahashi T., Matsui M., Seto H., Ono T., Kurachi M. Male-specific volume expansion of the human hippocampus during adolescence (2005). Cereb Cortex 15:187-93.

Svennerholm L., Bostrom K., Jungbjer B. Changes in weight and compositions of major membrane components of human brain during the span of adult human life of Swedes (1997). Acta Neuropathol 94:345-52.

Takashima H., Takebayashi T., Yoshimoto M., Terashima Y., Tsuda H., Ida K., Yamashita T. Correlation between T2 relaxation time and intervertebral disk degeneration (2012). Skeletal Radiol 41:163-7.

Takatalo J., Karppinen J., Niinimaki J., Taimela S., Nayha S., Mutanen P., Sequeiros R.B., Kyllonen E., Tervonen O. Does lumbar disc degeneration on magnetic resonance imaging associate with low back symptom severity in young Finnish adults? (2011). Spine (Phila Pa 1976) 36:2180-9.

Tertti M., Paajanen H., Laato M., Aho H., Komu M., Kormano M. Disc degeneration in magnetic resonance imaging. A comparative biochemical, histologic, and radiologic study in cadaver spines (1991). Spine (Phila Pa 1976) 16:629-34.

Tofts P. (2005) Quantitative MRI of the Brain : Measuring Changes Caused by Disease Wiley Imprint John Wiley & Sons, Hoboken.

Toth A., Kovacs N., Perlaki G., Orsi G., Aradi M., Komaromy H., Ezer E., Bukovics P., Farkas O., Janszky J., Doczi T., Buki A., Schwarcz A. Multi-modal magnetic resonance imaging in the acute and sub-acute phase of mild traumatic brain injury: can we see the difference? (2013). J Neurotrauma 30:2-10.

Trattnig S., Stelzeneder D., Goed S., Reissegger M., Mamisch T.C., Paternostro-Sluga T., Weber M., Szomolanyi P., Welsch G.H. Lumbar intervertebral disc abnormalities: comparison of quantitative T2 mapping with conventional MR at 3.0 T (2010). Eur Radiol 20:2715-22.

Urban J.P., McMullin J.F. Swelling pressure of the lumbar intervertebral discs: influence of age, spinal level, composition, and degeneration (1988). Spine (Phila Pa 1976) 13:179-87.

van der Toorn A., Sykova E., Dijkhuizen R.M., Vorisek I., Vargova L., Skobisova E., van Lookeren Campagne M., Reese T., Nicolay K. Dynamic changes in water ADC, energy metabolism, extracellular space volume, and tortuosity in neonatal rat brain during global ischemia (1996). Magn Reson Med 36:52-60.

van Graan L.A., Lemieux L., Chaudhary U.J. Methods and utility of EEG-fMRI in epilepsy (2015). Quant Imaging Med Surg 5:300-12.

Van Paesschen W., Connelly A., Johnson C.L., Duncan J.S. The amygdala and intractable temporal lobe epilepsy: a quantitative magnetic resonance imaging study (1996). Neurology 47:1021-31.

Vermeer S.E., Hollander M., van Dijk E.J., Hofman A., Koudstaal P.J., Breteler M.M., Rotterdam Scan S. Silent brain infarcts and white matter lesions increase stroke risk in the general population: the Rotterdam Scan Study (2003). Stroke 34:1126-9.

Viera A.J., Garrett J.M. Understanding interobserver agreement: the kappa statistic (2005). Fam Med 37:360-3.

Villanueva V., Serratosa J.M. Temporal lobe epilepsy: clinical semiology and age at onset (2005). Epileptic Disord 7:83-90.

Wagner J., Weber B., Urbach H., Elger C.E., Huppertz H.J. Morphometric MRI analysis improves detection of focal cortical dysplasia type II (2011). Brain 134:2844-54.

Wang C., Witschey W., Goldberg A., Elliott M., Borthakur A., Reddy R. Magnetization transfer ratio mapping of intervertebral disc degeneration (2010). Magn Reson Med 64:1520-8.

Watanabe A., Benneker L.M., Boesch C., Watanabe T., Obata T., Anderson S.E. Classification of intervertebral disk degeneration with axial T2 mapping (2007). AJR Am J Roentgenol 189:936-42.

Wattjes M.P., Steenwijk M.D., Stangel M. MRI in the Diagnosis and Monitoring of Multiple Sclerosis: An Update (2015). Clin Neuroradiol 25 Suppl 2:157-65.

Wehner T., Luders H. Role of neuroimaging in the presurgical evaluation of epilepsy (2008). J Clin Neurol 4:1-16.

Whitcher B., Schmid V., Thornton A. Working with the DICOM and NIfTI Data Standards in R (2011). Journal of Statistical Software 44:1-29.

Whittall K.P., MacKay A.L., Graeb D.A., Nugent R.A., Li D.K., Paty D.W. In vivo measurement of T2 distributions and water contents in normal human brain (1997). Magn Reson Med 37:34-43.

Whittall K.P., MacKay A.L., Li D.K., Vavasour I.M., Jones C.K., Paty D.W. Normal-appearing white matter in multiple sclerosis has heterogeneous, diffusely prolonged T(2) (2002). Magn Reson Med 47:403-8.

Wood E.T., Ronen I., Techawiboonwong A., Jones C.K., Barker P.B., Calabresi P., Harrison D., Reich D.S. Investigating axonal damage in multiple sclerosis by diffusion tensor spectroscopy (2012). J Neurosci 32:6665-9.

Yu L.P., Qian W.W., Yin G.Y., Ren Y.X., Hu Z.Y. MRI assessment of lumbar intervertebral disc degeneration with lumbar degenerative disease using the Pfirrmann grading systems (2012). PLoS One 7:e48074.

Yu S.W., Sether L.A., Ho P.S., Wagner M., Haughton V.M. Tears of the anulus fibrosus: correlation between MR and pathologic findings in cadavers (1988). AJNR Am J Neuroradiol 9:367-70.

Zhang Y., Brady M., Smith S. Segmentation of brain MR images through a hidden Markov random field model and the expectation-maximization algorithm (2001). IEEE Trans Med Imaging 20:45-57.

Zobel B.B., Vadala G., Del Vescovo R., Battisti S., Martina F.M., Stellato L., Leoncini E., Borthakur A., Denaro V. T1rho magnetic resonance imaging quantification of early lumbar intervertebral disc degeneration in healthy young adults (2012). Spine (Phila Pa 1976) 37:1224-30.

Zou J., Yang H., Miyazaki M., Morishita Y., Wei F., McGovern S., Wang J.C. Dynamic bulging of intervertebral discs in the degenerative lumbar spine (2009). Spine (Phila Pa 1976) 34:2545-50.

Zuo J., Saadat E., Romero A., Loo K., Li X., Link T.M., Kurhanewicz J., Majumdar S. Assessment of intervertebral disc degeneration with magnetic resonance single-voxel spectroscopy (2009). Magn Reson Med 62:1140-6.